

Anonymous Referee #1

Received and published: 18 April 2018

The authors use the GEOS-5 chemical forecast system to simulate the CO distribution and the timing of CO enhancements observed during the Atom-1 aircraft mission in July-August 2016, using tagged CO tracers to attribute modelled CO to non-biomass burning and biomass burning (BB) sources from different regions. The authors also use multi-year satellite measurements (MOPITT and MODIS) of CO and AOD to verify if August 2016 is representative of typical boreal summer conditions. One of the goals of Atom is to derive a chemical climatology over the ocean. The paper is well written and the authors have conveyed their results and findings clearly. The methods used to derive the results are sound and thorough. I recommend this paper to be published with some clarification and improvements, detailed below.

**We thank the referee for the positive review and respond to specific comments below.**

Specific comments

1. My major concern is that the authors combined BB emissions from Europe and from Northern Asia into one tagged CO tracer, which I think leads to difficult attributions of the simulated North Atlantic CO to emissions in these two regions. One would suspect that European BB emissions have a more direct impact on North Atlantic CO peaks than the Asian BB emissions. Moreover, the text seems to imply that BB emissions from Southern Asia and Australia are not included in the simulation, which might lead to the underestimation of simulated South Pacific CO peaks.

**We agree that it would be helpful to separate European and northern Asian BB emissions. However, since we used the GEOS-fp system, we are constrained to use the tagged-CO region definitions used by the fp system, and the fp system combines European and northern Asian BB emissions into one tracer. BB emissions from Southern Asia and Australia are included in the simulation, just not in the Eurasian tracer. They are included in the “Other BB” tracer instead. We clarify this by adding the following line to the caption of Table 1: “Other BB does include southern Asia as well Australia.” We also added a supplemental figure that shows the definition of each tagged tracer region on a map.**

2. Can you add to the map showing the ATom flight route the names of locations mentioned in the text and the labels of flight numbers?

**We added a supplemental figure showing the ATom flight route with locations and flight numbers labeled.**

3. L116-118: How do you justify adding 20% fossil fuel and 11% BB to CO emissions? What is the basis, and do you have a reference for the scaling factors? Please also show the effective CO total emissions, after scaling, in Table 1.

**We include these scalings to account for CO production from VOCs because VOCs are often emitted along with CO from fossil fuel and BB sources, but the GEOS-fp chemical mechanism does not carry VOCs and thus does not explicitly calculate the CO production from these co-emitted VOCs. The reference for these scaling factors is Duncan et al. [2007]. We add the following explanation to the text:**

**“...since VOC’s are not explicitly carried in the GEOS-fp chemical mechanism. This approach was developed by *Duncan et al. (2007)* to account for the CO source from non-methane hydrocarbon oxidation.” We added the effective CO emissions to Table 1 as suggested.**

4. L119-120: Which regions? Methane is well-mixed, and is oxidised in all regions. Could you clarify?

**The regions depend on where oxidation occurs, not where the methane is emitted. Thus, if methane is oxidized over Asia, the resulting CO is included in the Asian non-BB tracer. If it is oxidized over North America, it is included in the North American non-BB tracer. We add the following example to the text:**

**“For example, if methane is oxidized over North America, the resulting CO is included in the North American non-BB tracer.”**

5. L152-154: Could you elaborate why the observed peaks in Figure 1d are not captured by the GEOS-5 analysis? Could it be due to the underestimation of Asian BB or/and non-BB in the inventory?

**Tagged tracers in Fig. 1g suggest that they are due to biomass burning, but this could be due to either insufficient emissions or insufficient model resolution.**

**We add the following text to Section 3.1.1: “Either biases in emissions or insufficient vertical or horizontal model resolution may thus be responsible for the underestimate. The tagged tracer for biomass burning shows a small increase at the time of the underestimated plumes near hour 22 of the Anchorage-Kona flight (Fig. 1d,g), suggesting that those underestimates are due to the insufficient magnitude of the simulated biomass burning plumes.”**

6. Did you include biomass burning from South Asia and Australia in your CO simulation?

If these are not included, would this lead to the underestimation of the peaks in observed CO in Figure 1f? This is related to the comment above.

**Yes, they are included. This is now clear from the new supplemental figure showing the tagged tracer region definitions.**

7. L194-196: It is somewhat surprising that this region has notable Asian non-BB influence; could it be the case that the majority of this influence originates from Europe or Central Asia rather than from the Far East?

**Non-BB CO from Europe is tagged separately so would not show up in the Asian non-BB tracer. We are not able to distinguish Central Asia from East Asia with the tagged tracers. However, the Asian non-BB contribution here, though notable, is not huge, and given the lifetime of CO it is not too surprising that the large Asian CO source would make some contribution to the background even here.**

8. L197-198 and Figure 2f: Would it more precise to attribute the observed CO plumes here to European BB? Could N. American BB contribute to the plumes? Separating European and Asian BB emissions could shed more light on this.

**The tagged tracers show little N. American BB contribution to these plumes. We agree that separate European and Asian BB tracers would help shed light on this, but as explained above, these are not available. Examination of the fire emissions from this time period shows fires in both Europe and Asia, making it difficult to separate the two.**

9. L212-213: “An underestimate of Eurasian biomass burning contributes to the model underestimates in the North Pacific and North Atlantic, : : :” – same comment as above.

**As noted above, we do not have the ability to separate the European and Asian biomass burning contributions.**

10. Figures 5 and 6: I suggest to use the same scale between the 2 panels in each figure.

**Done.**

11. L364-369: The negative trends are not necessarily associated with the lower than average value of 2016. Often, IAV is larger than the trend. Whether 2016 is extreme or not should be defined based on statistical metrics.

**We agree that IAV can exceed the trend. The purpose of this discussion is just to point out previous work that shows a trend in MOPITT, and that this can be one factor contributing to the low values in 2016. It is also relevant to the 2<sup>nd</sup> referee’s question about MOPITT drift.**

**We add the following clarification:**

**This negative trend may be contributing to the low values in 2016, “although there is also substantial IAV in CO.”**

Technical corrections

1. L22: add “boreal” before “summer”

**Done**

2. L293: replace “summer” with “boreal summer/austral winter”

**Done**

3. L335: replace “autumn” with “September to November”

**We now say September-October, since this is when ATom-3 took place.**

4. Figure 8: please tidy up the label on the x-axis.

**Fixed**

5. Figures 11 and 12: please add “August” in the caption.

**Done**

6. Table S1: flights are labelled from 0 to 10 – should it be 1-11?

**Yes, we updated the numbering to be 1-11.**

Anonymous Referee #2

Received and published: 19 April 2018

General Comments

A very unique set of measurements obtained during the ATom-1 mission was analyzed throughout this study. Comprehensive data sets, both from in-situ and satellites, and a state-of-the-art global chemistry model were utilized. The analyses methods used here were reasonable and the results are presented in logical manner. However, it is not clear to me that what the scientific backgrounds are and what scientific questions the authors try to answer. What new and unique findings are discussed in this study? What can we learn from the results presented here? Specifically, why is it important for GEOS-5 to be able to simulate and forecast CO over the ocean? And why ATom-1 (and also the future deployment phases) was planned and how is it different from the previous campaigns, for instance, HIPPO? I think including more scientific background and contexts, and specific goals will make this article far more interesting.

**We thank the referee for the thoughtful comments. We have expanded the introduction to**

include some of the goals of ATom and relate our modeling work to those goals. In particular, we now state: “Major goals of the Atom mission include identifying chemical processes that control the concentrations of short-lived climate forcers, quantifying how anthropogenic emissions affect chemical reactivity globally, and identifying ways to improve the modeling of these processes” and “GEOS-5 forecasts help determine the source regions and emission types that contribute to the trace gas and aerosol concentrations measured during ATom, which is directly relevant to the goal of quantifying how anthropogenic emissions affect global chemical reactivity.” We also clarify the importance of validating GEOS-5, adding “GEOS-5 supports numerous aircraft missions, and validation of the model forecasts is important for developing confidence in and understanding the limitations of chemistry forecasting for aircraft missions. The ATom dataset, which uses unbiased sampling rather than chasing plumes, provides a unique opportunity to validate the overall performance of the GEOS-5 model on a global scale.”

We also added a supplemental figure showing a map of the ATom flight tracks.

In the future, the ATom Mission PI will prepare an overview paper that contains more details on the scientific background, planning, goals, and overall accomplishments of ATom. An extensive discussion of these topics is thus beyond the scope of the present work.

#### Specific Comments

P1 (Abstract) – I think the abstract can be rewritten in order for it to serve as a brief summary of this study. The simplest way is to rearrange it. 1) What is the goal of ATom-1, 2) What are the observational findings shown in this study, 3) Why is the modeling study performed and 4) What the conclusion is.

We reorganized the abstract to begin with a description of ATom and better motivate our modeling study. We add “The first phase of the Atmospheric Tomography Mission (ATom-1) took place in July-August of 2016 and included flights above the remote Pacific and Atlantic oceans. Sampling of atmospheric constituents during these flights is designed to provide new insights into the chemical reactivity and processes of the remote atmosphere and how these processes are affected by anthropogenic emissions. Model simulations provide a valuable tool for interpreting these measurements and understanding the origin of the

**observed trace gases and aerosols, so it is important to quantify model performance” and “We use GEOS-5’s tagged tracers for CO to assess the contribution of different emission sources to the regions sampled by ATom-1 to elucidate the dominant anthropogenic influences on different parts of the remote atmosphere”.**

P2 (Introduction) – This section can be rewritten to add clarity as well. It should include 1) Scientific background and goals of the ATom-1 (and other phases) mission, 2) What are the scientific questions ATom-1 aimed to answer? 3) What did ATom-1 sample and accomplish? 4) What is the goal of this study?

**We have expanded the introduction as described in the response to General Comments to include information on the goals of ATom and how our work relates to these goals. We also added a link to the ATom website, which includes additional information about ATom.**

In addition, the information in the third and the fourth paragraphs (lines 42-53) provides general overview, instead of specific to this study.

**We reorganized this section to better link the overview to the current study.**

I would also like to know what the ATom-1 specific references are. Is Prather et al. (2017) the only reference relevant to ATom-1?

**We also reference the doi for the ATom dataset. We added a reference to *Prather et al. [2018]* to Section 5.**

Technical Comments

P3 (Section 2.1) – What are the vertical ranges of ATom-1 measurements? The accuracy or precision of the species measured during ATom-1 should be provided here.

**We state that “Each of the 11 flights included sampling from the boundary layer to the top of the aircraft range (39 kft).” The QCLS observations have an accuracy and precision of 3.5 ppb and 0.15 ppb, respectively. We added that statement to this section.**

P3 (Section 2.2) – The vertical range of MOPITT and MLS and their overlap have to be mentioned specifically. What pressure ranges do they overlap?

**We now clarify that we are using the CO column and 700 hPa CO retrievals from MOPITT and the 215 hPa level for MLS. We also add the following about the overlap: “The MOPITT averaging kernels include some sensitivity to the 200 hPa level, implying a small overlap between the MOPITT and MLS observations.”**

How often did ATom-1 sample stratosphere? Are there any ground-based measurements to compare? It has to be mentioned why only the satellite data are used in the comparison. Also, why was the MODIS AOT used?

**We use satellite observations for our analysis of interannual variability because they provide broad spatial coverage over the oceans, where most of the ATom sampling occurred. Ground-based measurements over the oceans are sparse, so we do not include them in this analysis. We use MODIS AOT to examine aerosol interannual variability because MODIS provides a relatively long record. We added text clarifying these points: “We focus on satellite observations because they provide broad coverage over the oceans, where surface data is sparse. “ “We use MODIS data in this analysis because it provides a relatively long data record.”**

P3 (MOPITT) – I believe the current version of MOPITT is 7 not 6.

**This is correct. We used version 6 in this study because it was a well-established product at the time we conducted this analysis.**

P4 (Section 2.3) – It has to be mentioned why the model is used in this study. What are the questions that can be answered through modeling? Is a global model the sufficient tool for this study?

**We added the purpose of the model to the first sentence and clarify that a global model is necessary because CO is transported globally. We added the following text about why we use GEOS-5:**



**“to quantify the contribution of different emission sources to the observed CO distribution and to identify the origin of observed plumes. A global model is necessary for this analysis since CO is transported globally.” and “We use the FP system in our study because it is the system used to generate forecasts that are used during ATom and other aircraft missions, and is thus relevant to future mission and flight planning.”**

P4 (L125) – What could be learned from the chemical forecasts during a field campaign, such as, ATom-1? How many pollution or non-pollution events occurred during the ATom-1 period?

**We add a discussion of what chemical forecasts tell us to the first paragraph of Section 3. Pollution plumes are shown in figures 1 and 2. We add this text to Section 3:**

**“The chemical forecasts provide the ATom team with a preview of the chemical environments that the flight is expected to sample, including the location of pollution, biomass burning, or dust plumes; regions of substantial but well-mixed anthropogenic pollution; and cleaner regions. The forecasts also provide a broader spatial context for the observations, since the 3-dimensional model output shows the spatial extent of features that intersect the flight track.”**

P5 (L160) – Is the bias in the emissions responsible for the underestimation in the model? What about the spatial resolution of the model?

**These are both possible explanations. We add the following clarification:**

**“Either biases in emissions or insufficient vertical or horizontal model resolution may thus be responsible for the underestimate.”**

P5 (L167) – ‘As expected from the basic chemistry and seen in previous observations’ can be replaced by ‘In the stratosphere’.

**We now say “As expected from stratospheric chemistry and seen in previous observations”**

P5 (L169) – ‘Underestimating the observed decrease’ can possibly be replaced by ‘showing higher CO’ or something similar.

**We changed it to “underestimating the observed gradient” since we want to convey that the change in CO as the flight enters the stratosphere is underestimated.**

P6 (L184)- The meaning if this sentence is unclear. So, using analysis and forecast wind fields makes no difference? Does this mean that the wind fields are the same or the results are not sensitive to the winds? And what is the reason for this?

**It means that the plume timings are already captured by the forecast winds and don’t change substantially with the analysis winds. We reword this sentence to say: “Comparison of Fig. S4 with Fig. 2f shows that the impact of using analysis versus forecast wind fields is small for this flight since the forecasts already capture the timing of the plumes.”**

P6 (L193 & L203) – What determines the placement of the plumes in the model? Do models misplace the plumes often?

**We added “extent” as well as placement of the plumes. In general, the good agreement in the timing of plumes in the model compared to observations suggests that the model usually places the plumes correctly. However, the placement of plumes is sensitive to vertical and horizontal transport, and to the injection height of the biomass burning emissions. The injection height is a source of uncertainty. In addition, global eulerian models tend to diffuse plumes too quickly. We added the following text to explain this:**

**“The placement and strength of simulated plumes is sensitive to the injection height of the biomass burning, which is a source of uncertainty. In addition, plumes in models tend to dissipate more quickly than in observations due to the numerical effects of limited model resolution (*Eastham and Jacob, 2017*).”**

P7 (Figure 4 description) – It is not easy to compare the data and the model simulations in this figure. I wonder what the differences (data-model, or %) would look like if it’s plotted like Fig. 4a and 4b.

**We added a third panel plotting the data – model difference.**

P9 (L306) – Full name for GFED version 4 and a citation should be included.

**We added the full name and the reference to *van der Werf et al.*, [2017]**

P9 (L312) – ‘its relative variability’ – what does this mean?

**Relative variability means the variability relative to the mean. We add this clarification to the text.**

P10 (L320) - A reference is needed for Siberian biomass burning here.

**We provide references later in this paragraph for large fires in western Russia and Siberia.**

P11 (L353-354) – Is this expected? And why?

**Both CO and aerosols have a major source from biomass burning, so it makes sense that regions influenced by biomass burning, such as the tropical Atlantic, would have high values of both CO and aerosols. We add the following:**

**“This similarity is consistent with the importance of biomass burning emissions for both CO and aerosols.”**

P11 (L366-367) - I wonder if and how the MOPITT V6 bias drift is accounted for in this study.

**We do not attempt to account for the MOPITT drift, except to mention it in the text. Since the drift in the CO column is almost negligible [*Deeter et al.*, 2014], we do not expect it to influence our CO column results. There may be a small impact from the drift on the 700 hPa results, but those results are generally consistent with the CO column results.**

P12 (L402) – A general website for the ATom mission will be useful to include here.

**We added a link to the ATom website in the introduction.**

P12 (references) – Formatting of the references should be corrected to be consistent with the publication standard.

**We have formatted the references in this way.**

P17 & 18 (Tables 1 & 2) – A map showing all the geographical regions (with specific latitude and longitude) used in Tables 1 & 2 might be useful. I am also curious to know if it would be easier to compare the observations and the model in a form of a bar graph instead of a table (Table 2).

**We added a supplemental figure showing maps of the geographical regions corresponding to the tagged tracers. We added another supplemental figure showing the ATom flight tracks on a map and labeling the start and end points of the flights, so that the reader can visualize the locations discussed in Table 2. We prefer to keep Table 2 as a table so that we can more easily and quantitatively compare the standard deviations as well as the mean values.**

P18 (Fig. 1) – I wonder what would Figs. 1d-1f and Figs 1g-1i would look like if they have the same vertical ranges. The current plots give a false impression that CO is higher between Kona-Pago Pago-Christchurch than the first leg.

**We considered this, but putting panel e on the same scale as panel d squashes the detail in panel d.**

1 **Forecasting Carbon Monoxide on a Global Scale for the**  
2 **ATom-1 Aircraft Mission: Insights from Airborne and**  
3 **Satellite Observations and Modeling**

4  
5 Sarah A. Strode<sup>1,2</sup>, Junhua Liu<sup>1,2</sup>, Leslie Lait<sup>2,3</sup>, Róisín Commane<sup>4</sup>, Bruce Daube<sup>4</sup>, Steven Wofsy<sup>4</sup>, Austin  
6 Conaty<sup>2,5</sup>, Paul Newman<sup>2</sup>, Michael Prather<sup>6</sup>

7  
8 <sup>1</sup>Universities Space Research Association, Columbia, MD, USA

9 <sup>2</sup>NASA GSFC, Greenbelt, MD, USA

10 <sup>3</sup>Morgan State University, Baltimore, MD, USA

11 <sup>4</sup>Harvard University, Cambridge, MA, USA

12 <sup>5</sup>SSAI, Greenbelt, MD, USA

13 <sup>6</sup>University of California, Irvine, CA, USA

14

15 *Correspondence to:* Sarah A. Strode (sarah.a.strode@nasa.gov)

16

17 **Abstract** The first phase of the Atmospheric Tomography Mission (ATom-1) took place in July-August of  
18 2016 and included flights above the remote Pacific and Atlantic oceans. Sampling of atmospheric  
19 constituents during these flights is designed to provide new insights into the chemical reactivity and processes  
20 of the remote atmosphere and how these processes are affected by anthropogenic emissions. Model  
21 simulations provide a valuable tool for interpreting these measurements and understanding the origin of the  
22 observed trace gases and aerosols, so it is important to quantify model performance. GEOS-5 forecasts and  
23 analyses show considerable skill in predicting and simulating the CO distribution and the timing of CO  
24 enhancements observed during the ATom-1 aircraft mission. We use GEOS-5's tagged tracers for CO to  
25 assess the contribution of different emission sources to the regions sampled by ATom-1 to elucidate the  
26 dominant anthropogenic influences on different parts of the remote atmosphere. We find a dominant  
27 contribution from non-biomass burning sources along the ATom transects except over the tropical Atlantic,  
28 where African biomass burning makes a large contribution to the CO concentration. One of the goals of  
29 ATom is to provide a chemical climatology over the oceans, so it is important to consider whether August  
30 2016 was representative of typical boreal summer conditions. Using satellite observations of 700 hPa and  
31 column CO from the Measurement of Pollution in the Troposphere (MOPITT) instrument, 215 hPa CO from  
32 the Microwave Limb Sounder (MLS), and aerosol optical thickness from the Moderate Resolution Imaging

**Deleted:** Using tagged tracers for CO, w

34 Spectroradiometer (MODIS), we find that CO concentrations and aerosol optical thickness in Aug. 2016  
35 were within the observed range of the satellite observations, but below the decadal median for many of the  
36 regions sampled. This suggests that the ATom-1 measurements may represent relatively clean but not  
37 exceptional conditions for lower tropospheric CO.

## 38 1 Introduction

39 The first phase of the NASA Atmospheric Tomography Mission (ATom-1)  
40 (<https://espo.nasa.gov/atom>) took place in July-August 2016. The aircraft completed a circuit beginning in  
41 Palmdale, California and traversing the remote Pacific and Atlantic oceans, providing an unprecedented  
42 picture of the chemical environment at a wide range of latitudes over the remote oceans. Major goals of the  
43 Atom mission include identifying chemical processes that control the concentrations of short-lived climate  
44 forcers, quantifying how anthropogenic emissions affect chemical reactivity globally, and identifying ways  
45 to improve the modeling of these processes.

46 Chemical forecasts from the GEOS-5 model provided insight into the chemical environments and  
47 sources of pollution for the diverse regions sampled during the ATom-1 campaign. GEOS-5 forecasts help  
48 determine the source regions and emission types that contribute to the trace gas and aerosol concentrations  
49 measured during ATom, which is directly relevant to the goal of quantifying how anthropogenic emissions  
50 affect global chemical reactivity. GEOS-5 supports numerous aircraft missions, and validation of the model  
51 forecasts is important for developing confidence in and understanding the limitations of chemistry forecasting  
52 for aircraft missions. The ATom dataset, which uses unbiased sampling rather than chasing plumes, provides  
53 a unique opportunity to validate the overall performance of the GEOS-5 model on a global scale.

54 One of the goals of ATom is to provide an observation-based climatology of important atmospheric  
55 constituents and their reactivity in the remote atmosphere. Consequently, it is important to examine whether  
56 the ATom observations are temporally and spatially representative of the broader remote atmosphere.  
57 *Prather et al. (2017)* examined the ability of observations from a single path to represent the variability of a  
58 broader geographic region, but noted that year-to-year and El Nino/Southern Oscillation (ENSO) variability  
59 could also be important. Year to year variability in meteorology and emissions both contribute to interannual  
60 variability in trace gases and aerosols, so it is important to consider the temporal representativeness of a  
61 single season sampled by ATom. For example, ENSO is a major driver of variability in ozone distributions  
62 (*Ziemke and Chandra, 2003*), and large biomass burning events during El Nino years increase concentrations  
63 of trace gases including CO and CO<sub>2</sub> (*Langenfelds et al., 2002*). Biomass burning plays a particularly strong  
64 role in driving the interannual variability of CO (e.g. *Novelli et al., 2003; Kasischke et al., 2005; Duncan and*  
65 *Logan, 2008; Stroe and Pawson, 2013; Voulgarakis et al., 2015;*). The impacts of large biomass burning  
66 events during El Nino events are visible in satellite observations of CO (e.g. *Edwards et al., 2004; Edwards*  
67 *et al., 2006; Logan et al., 2008, Liu et al., 2013*). *Pfister et al. (2010)* used a chemistry transport model (CTM)  
68 as well as satellite data to examine the CO sources and transport over the Pacific during the INTEX-B mission  
69 compared to previous years. They found biomass burning to be the largest contributor to interannual

Deleted: s

Formatted: Indent: First line: 0"

Deleted:

Moved down [1]: Here we show how the time and place of ATom-1 measurements fit into a global, multi-year climatology of CO.

Deleted: ¶

Deleted: ¶

77 variability, despite its lower emissions compared to fossil fuel sources. [Here we show how the time and place](#)  
78 [of ATom-1 measurements fit into a global, multi-year climatology of CO. In particular, we assess the extent](#)  
79 [to which measurements from the ATom-1 period represent the CO and aerosol distributions over the last](#)  
80 [decade and a half.](#)

Moved (insertion) [1]

81 In this study, we place the August 2016 ATom observations in the context of interannual variability and  
82 assess the contributions of different emission sources to the various regions sampled during the campaign.  
83 We focus on CO, a tracer of incomplete combustion whose lifetime of 1-2 months allows long-range transport  
84 to the remote oceans. Section 2 describes the model and observations used in this analysis. Section 3  
85 compares the GEOS-5 CO to observations. Section 4 discusses the global distribution of CO, and presents  
86 the relative CO source contributions to the regions sampled by ATom. Section 5 presents an analysis of the  
87 interannual variability in CO and aerosol optical thickness seen in satellite observations to assess how well  
88 August 2016 observations represent climatological August conditions. Section 6 summarizes our  
89 conclusions.

## 90 2 Observations and Model

### 91 2.1 ATom Observations

92 ATom-1 flew transects through the Pacific, Southern, Atlantic and Arctic oceans with the NASA DC8  
93 aircraft in August 2016. Each of the 11 flights included sampling from the boundary layer to the top of the  
94 aircraft range (39 kft). We use the ATom-1 data (July-August 2016) [*Atom Science Team, 2017*] for  
95 comparison with the model forecasts and analyses.

96 We take ATom-1 CO observations from the Harvard QCLS instrument (*Santoni et al., 2014*), which  
97 has a history of successful measurements during the HIAPER Pole-to-Pole Observations (HIPPO) campaign.  
98 Briefly, the instrument uses a pulsed quantum cascade laser at  $2160\text{ cm}^{-1}$  to measure absorption of CO through  
99 a astigmatic multi-pass sample cell (with 76 m path length), with detection using liquid nitrogen cooled  
100 HgCdTe detector. A separate laser and detector are used to measure methane and nitrous oxide in the same  
101 cell. Inflight calibrations were conducted with gases traceable to the NOAA WMO (X2014) scale, with  
102 calibration of tanks before ATom1 and after ATom2 (February 2017) showing no significant change in the  
103 CO concentration in the gas standards. The inlet for the instrument was specially designed for the DC-8  
104 aircraft. [The QCLS observations have an accuracy and precision of 3.5 ppb and 0.15 ppb, respectively. The](#)  
105 [QCLS observations used in this analysis are being archived at the ORNL DAAC](#)  
106  [\(https://doi.org/10.3334/ORNLDAAC/1604\).](https://doi.org/10.3334/ORNLDAAC/1604)

### 108 2.2 Satellite Observations

109 We use satellite observations that cover more than a decade to examine the interannual variability  
110 of CO and aerosols. [We focus on satellite observations because they provide broad coverage over the oceans.](#)

111 [where surface data is sparse](#). The Measurement of Pollution in the Troposphere (MOPITT) instrument, which  
112 flies on the Terra satellite, provides CO observations beginning in 2000 (*Edwards et al.*, 2004). We use the  
113 version 6 thermal infrared (TIR) level 3 product (*Deeter et al.*, 2014). The MOPITT TIR averaging kernels  
114 show high sensitivity to CO between 700 and 500 hPa (*Emmons et al.*, 2007). [We use the CO column and](#)  
115 [700 hPa CO retrievals](#).

116 The Microwave Limb Sounder (MLS) (*Waters et al.*, 2006), which flies on the Aura satellite,  
117 provides useful observations of CO down to 215 hPa (*Livesey et al.*, 2008) beginning in 2004. We use the  
118 Version 4.2 level 2 data [for the 215 hPa level](#) with the recommended quality, status, precision, and  
119 convergence criteria. Although MLS data overlap with ATom only at the highest flight levels, both it and  
120 MOPITT provide complementary views of CO in the lower troposphere and upper troposphere/lower  
121 stratosphere (UTLS), respectively. [The MOPITT averaging kernels include some sensitivity to the 200 hPa](#)  
122 [level, implying a small overlap between the MOPITT and MLS observations](#).

123 The Moderate Resolution Imaging Spectroradiometer (MODIS) instrument on the Aqua satellite  
124 provides column aerosol optical thickness (AOT) data beginning in 2002. [We use MODIS data in this](#)  
125 [analysis because it provides a relatively long data record](#). We use the Collection-6 level 2 (MYD04\_L2)  
126 [*Levy et al.*, 2015] 550 nm AOT data over oceans aggregated into 0.5 degree grid boxes, and then take  
127 monthly means with the daily data weighted according to the QA.

### 128 2.3 Model Description

129 We use chemical forecasts and analyses from the GEOS-5 Forward Processing (FP) system [to](#)  
130 [quantify the contribution of different emission sources to the observed CO distribution and to identify the](#)  
131 [origin of observed plumes. A global model is necessary for this analysis since CO is transported globally](#).  
132 The FP stream from the Global Modeling and Assimilation Office (GMAO) generates GEOS-5 forecast  
133 products as well as assimilation products using the most current system approved for near-real-time  
134 production. [We use the FP system in our study because it is the system used to generate forecasts that are](#)  
135 [used during ATom and other aircraft missions, and is thus relevant to future mission and flight planning](#). The  
136 GEOS-5 model (*Molod et al.*, 2015) is a global general circulation model (GCM) with 72 vertical levels  
137 reaching from the surface to 1 Pa. The assimilation system is described in (*Rienecker et al.*, 2008; *Rienecker*  
138 *et al.*, 2011), and includes assimilation of ozone measurements from the Ozone Monitoring Instrument (OMI)  
139 and MLS, and aerosol optical depth as well as meteorological variables. The forward processing system  
140 produces output on 72 model levels or 42 pressure levels with 5/16 by 1/4 degree horizontal resolution. Our  
141 study uses the pressure level output.

142 The GEOS-5 FP system (*Lucchesi*, 2017) simulates the transport of CO as well as tagged CO tracers  
143 from specific regions and sources, which helps track the transport of pollution outflow. Tagged tracers are  
144 available for biomass burning (BB) globally as well as biomass burning from Eurasia, North America, Africa,  
145 and Central and South America; and for non-BB sources globally and from Europe, Asia, and North America.  
146 Non-BB sources include fossil fuels, biofuels, CO from oxidation of biogenic VOCs, and CO from methane



147 oxidation, as described in *Ott et al.* (2010). [Supplemental Figure S1 shows the regions included in each](#)  
148 [tagged tracer.](#) *Bian et al.* (2013) used observations of dichloromethane and acetonitrile from the ARCTAS  
149 mission to validate the anthropogenic and biomass burning CO tracers, respectively.

150 Daily-varying biomass burning emissions come from the Quick Fire Emission Dataset (QFED)  
151 version 2 [*Darmenov and da Silva*, 2015], which is based on fire radiative power from the MODIS  
152 instrument. Thus the BB emissions include day-to-day and interannual variability, but the non-BB sources  
153 and the OH fields use monthly means and lack daily-scale variability and interannual variability. Table 1  
154 presents the August emission inputs for the major regions considered. CO emissions are then scaled up by  
155 20% for fossil fuels and 11% for biomass burning to account for CO production from co-emitted VOCs, [since](#)  
156 [VOC's are not explicitly carried in the GEOS-fp chemical mechanism. This approach was developed by](#)  
157 [Duncan et al. \(2007\) to account for the CO source from non-methane hydrocarbon oxidation.](#)

158 CO from methane oxidation is included in the non-BB tagged tracers for the regions in which  
159 oxidation occurred. [For example, if methane is oxidized over North America, the resulting CO is included](#)  
160 [in the North American non-BB tracer.](#) The monthly mean methane fields come from a GMI Chemistry and  
161 Transport Model (CTM) simulation, which uses prescribed zonal mean surface concentrations. CO is lost  
162 by reaction with OH using fixed monthly OH fields archived from the GMI CTM. Supplemental Figure S2  
163 shows the methane and OH fields included in the FP system.

### 164 3 GEOS-5 Chemical Forecasting for ATom

165 During the ATom mission, the GEOS-5 model is engaged to provide chemical forecasts for each flight  
166 that include the major chemical species and, for CO, tagged tracers for different sources. The chemical  
167 forecasts are used together with meteorological forecasts for day-to-day flight planning, although flight tracks  
168 were intentionally not altered to chase specific chemical features to avoid a highly biased sampling of  
169 pollution. [The chemical forecasts provide the ATom team with a preview of the chemical environments that](#)  
170 [the flight is expected to sample, including the location of pollution, biomass burning, or dust plumes; regions](#)  
171 [of substantial but well-mixed anthropogenic pollution; and cleaner regions. The forecasts also provide a](#)  
172 [broader spatial context for the observations, since the 3-dimensional model output shows the spatial extent](#)  
173 [of features that intersect the flight track.](#)

174 We examine the performance of the GEOS-5 forecasts by comparing the simulated CO to the QCLS  
175 observations. The forecasts provided during the mission used forecast wind fields, with the forecast lead  
176 time varying depending on the timing of the flight. For consistency, the results shown here use the CO  
177 simulated with the assimilated wind fields, but we note that similar features were seen for the CO simulated  
178 with the forecast winds, as further discussed in section 3.1.2. For the model results, we do not apply temporal  
179 interpolation between the model output frequency (6 hours). Instead, we sample the model forecasts at the  
180 time closest to the mid-point of each flight segment. To compare with observations, the 3D model forecast  
181 was interpolated to the longitude, latitude and pressure given in the 10-second merges of the ATom  
182 measurements.

Deleted: ¶

Formatted: Indent: First line: 0.4"

Formatted: Font: 10 pt, Not Bold

Deleted: 1

185 **3.1 Analysis of CO along the Meridional Flight Tracks**

186 We compare CO from GEOS-5 to the QCLS CO observations for specific flights, using the 10-  
187 second merge files. The GEOS-5 CO is taken from the 3D field at the time closest to the mid-point of the  
188 flight and interpolated in space to the flight track. [The ATom flight tracks are shown in Supplemental Figure](#)  
189 [S3](#). We focus on two sections of the ATom-1 circuit: the North to South flights through the Pacific, and the  
190 South to North flights through the Atlantic, although we briefly discuss the other flights as well. These two  
191 transects allow us to examine the transition from northern hemispheric to tropical to southern hemispheric  
192 influence.

193 **3.1.1 Pacific legs**

194 Figure 1 shows CO from the three Pacific flights spanning Anchorage, Alaska to Christchurch, New  
195 Zealand. The top panels show the GEOS-5 curtain of CO along the flight track, with the QCLS observations  
196 overplotted in circles. The observations show higher values of CO in the first half of the Anchorage-Kona  
197 flight compared to the other portions of the Pacific, and this feature is reproduced in GEOS-5 as well. GEOS-  
198 5 agrees well with the observed mean value for CO on this flight (Table 2). Tagged tracers (Fig. 1 bottom  
199 panels) show that non-BB sources, especially from Asia, are the dominant contributor to CO levels  
200 throughout the Pacific, and the decrease in Asian non-BB CO explains the observed decrease in CO as the  
201 flights move south.

202 The observations show plumes of enhanced CO scattered throughout all three Pacific flights,  
203 although they are most intense in the north Pacific, as seen in the Anchorage-Kona flight. GEOS-5 typically  
204 reproduces the timing of these plumes, but the magnitude is usually underestimated, particularly for the  
205 strongest plumes. This leads to an underestimate of the observed standard deviation of the CO on the  
206 Palmdale-Anchorage (Fig. S4) and Anchorage-Kona flights (Table 2). In addition to biases in emissions,  
207 observations often show fine-scale structures too small for the model to resolve (Hsu et al., 2004), and  
208 underestimating the concentrations in strong plumes is a common problem for global models (e.g. *Heald et*  
209 *al.*, 2003). [Either biases in emissions or insufficient vertical or horizontal model resolution may thus be](#)  
210 [responsible for the underestimate. The tagged tracer for biomass burning shows a small increase at the time](#)  
211 [of the underestimated plumes near hour 22 of the Anchorage-Kona flight \(Fig. 1d,g\), suggesting that those](#)  
212 [underestimates are due to the insufficient magnitude of the simulated biomass burning plumes.](#) An exception  
213 is in the tropical Pacific (Kona-Pago Pago flight), in which GEOS-5 predicted some enhancements, driven  
214 by fossil fuels, not seen in the observations. Tagged tracers indicate that Asian non-BB CO drove many of  
215 the observed enhancements, while others were due to biomass burning.

216 In the south Pacific (Pago Pago to Christchurch segment), the flight sampled the stratosphere three  
217 times, with CO levels decreasing to approximately 30 ppb, as shown in Fig. 1c. As expected from  
218 [stratospheric](#) chemistry and seen in previous observations, both ATom-1 and GEOS-5 show a strong decrease  
219 in CO as the flight rises above the tropopause, with GEOS-5 underestimating the observed [gradient](#). Both  
220 the model and measurements show tropospheric CO less than 90 ppbv along the flight route with slightly

Deleted: 2

Deleted: the basic

Deleted: decrease

224 elevated CO above 600 hPa around T22:00 and T24:00. For this flight and the subsequent flight to Punta  
225 Arenas, all observations are in the Southern Hemisphere and the mean values for both ATom-1 and GEOS-  
226 5 agree within the range 54-57 ppb (Table 2, Fig S5).

Deleted: 3

### 227 3.1.2 Atlantic Legs

228 The ATom flights traversed the Atlantic from South to North, beginning in Punta Arenas, Chile and  
229 ending in Kangerlussuaq, Greenland. Figure 2 shows the Atlantic flights from Punta Arenas to Ascension  
230 Island to the Azores to Kangerlussuaq. GEOS-5 has an excellent simulation of background CO values seen  
231 on these flights, with the mean values falling within 2 ppb of the observations (Table 2) while the mean  
232 observed values for each flight shift from 69 to 101 to 88 ppb. The observations show plumes of high CO  
233 intersecting the flight track on all three flights. GEOS-5 also shows plumes of enhanced CO at these  
234 locations, but the magnitude is often underestimated (Fig. 2d-f), especially for the Azores-Kangerlussuaq  
235 flight. Supplemental Figure S6 shows the CO results for the Azores-Kangerlussuaq flight using forecast  
236 wind fields, and illustrates the temporal evolution of CO plumes along the flight track. Comparison of Fig.  
237 S6 with Fig. 2f shows that the impact of using analysis versus forecast wind fields is small for this flight  
238 since the forecasts already capture the timing of the plumes.

Deleted: 4

Deleted: 4

Deleted: the small

239 Non-BB sources dominate the background CO levels on all three flights. However, biomass burning  
240 plays a dominant role in the plumes of high CO (Fig. 2g-i). South American biomass burning leads to CO  
241 enhancements between T14 and T16 of the Punta Arenas to Ascension flight. In the later portion of that  
242 flight, biomass burning from Africa leads to strong CO plumes. Strong plumes of African biomass burning  
243 are also seen at the beginning of the Ascension to Azores flight. GEOS-5 shows a strong plume around 800  
244 hPa for the first hour of the flight, which agrees well with observations (Fig. 2b,d). The observations show  
245 additional strong plumes in the next hour between 600 and 700 hPa. These plumes are present but  
246 underestimated in GEOS-5, possibly due to errors in the magnitude of the emissions or the placement or  
247 extent of the plumes. The placement and strength of simulated plumes is sensitive to the injection height of  
248 the biomass burning, which is a source of uncertainty. In addition, plumes in models tend to dissipate more  
249 quickly than in observations due to the numerical effects of limited model resolution (Eastham and Jacob,  
250 2017).

251 The non-BB contribution to CO in the Atlantic reflects a mixture of global sources. Asian sources  
252 make a notable contribution to the non-BB CO variability in the tropics (first half of the Ascension to Azores  
253 flight), but as expected N. American sources become more dominant in the second half. In the northern  
254 (later) portion of the Azores to Kangerlussuaq flight (Fig. 2), GEOS-5 attributes the observed plumes to  
255 Eurasian biomass burning, but underestimates their magnitude. This flight also crosses the tropopause, and  
256 both ATom-1 and GEOS-5 show a corresponding dip in CO concentrations. GEOS-5 predicts a plume of  
257 enhanced CO due to N. American emissions around 11Z of the Azores to Kangerlussuaq flight that is not  
258 seen in the observations (Fig. 2f,i). A similar error is made in the Kangerlussuaq to Minneapolis flight (Fig.  
259 S5). This could be due to either an error in the assumed N. American sources, or to misplacement of the

Deleted:

Deleted: 3

266 plume by the model. A large overestimate of CO at the end of the Minneapolis to Palmdale flight also points  
267 to a potential error in North American emissions from either fossil fuels or biomass burning.

### 268 3.2 Model Evaluation Summary

269 We summarize the comparison between the CO simulated by the GEOS-5 analyses and the QCLS  
270 observations in Figure 3. The majority of points lie near the one-to-one line, indicating good overall  
271 agreement between the GEOS-5 and observed CO distributions. The higher concentrations in the tropical  
272 Atlantic compared to the tropical Pacific are evident in both the observations and model. Fig. 3 also reveals  
273 occasional model overestimates of CO on flights over North America (green triangles), as well as  
274 underestimates of high CO plumes over the North Pacific and Tropical Atlantic. An underestimate of  
275 Eurasian biomass burning contributes to the model underestimates in the North Pacific and North Atlantic,  
276 and has implications for ozone production in aged BB plumes [*Liu et al.*, in prep]. Globally, the correlation  
277 of simulated and observed CO with 5-minute binning is  $r=0.69$ . Correlations for the Pacific, Atlantic, and  
278 North America are 0.72, 0.80, and 0.80, respectively, while the correlation for the southern ocean is 0.053.  
279 The poor correlation for the southern ocean reflects the very low variability of CO in this region. The model  
280 performs far better at capturing the larger gradients present in the other regions. In general, the good  
281 agreement between model outputs and observations testify the model forecasting skill and suggest the  
282 suitability of using GEOS-5 forecast products to guide the design and execution of aircraft campaigns.

## 283 4 Source Contributions to the Global CO Distribution

### 284 4.1 Global CO Distribution

285 Figure 4 compares CO from GEOS-5 to the QCLS CO observations for the ATom-1 circuit including  
286 the 11 total flight segments. The GEOS-5 CO is taken from the analysis closest to the mid-point of the flight  
287 time and interpolated to the flight track following the longitude, latitude and pressure given in the  
288 observations. We average both model CO and ATom measurements into one point per 360-seconds for easier  
289 visualization.

290 Both model simulations and measurements show polluted air with higher CO mixing ratios in the  
291 northern hemisphere than that in the southern hemisphere in August 2016. Over the northern hemispheric  
292 polar region, the observations indicate highly polluted air with CO maxima occurring over Alaska and  
293 northwest Canada, features also seen in the GEOS-5 simulation. Over the Atlantic section, CO maxima with  
294 slightly lower values occur around the same latitude over west Greenland as shown both in observations and  
295 model simulation. CO over the northern most locations along the ATom-1 circuit see some low values both  
296 in model and observations, particularly north of 30°N and south of 40°S, due to the measurements occurring  
297 in the stratosphere or occurring in the upper troposphere with stratospheric influence. Both model and  
298 observations indicate that the air is relatively clean over the Pacific south of 30N with CO less than 70 ppb  
299 and the CO minimum around 60S over the southeast Pacific. Over the Atlantic section, both model and

300 observations show low CO concentration south of 30S, but show a strong CO maximum over the tropical  
301 Atlantic (5S-5N) with CO greater than 120 ppb. This high CO is mainly driven by southern hemisphere BB.  
302 CO is slightly lower between 30N and 60N compared to that over tropical Atlantic and the Greenland. The  
303 similarity between GEOS-5 and ATom-1 variability in neighboring points is due in part to the vertical  
304 profiling which places horizontally extensive biomass burning layers in both model and presumably the  
305 atmosphere at the same point along the track.

#### 306 4.2 CO Source Contributions

307 We calculate the contribution of different CO sources to the total simulated CO using the GEOS-5  
308 tagged CO tracers sampled along the ATom flight tracks. This analysis provides a picture of the dominant  
309 sources affecting the constituent concentrations observed during ATom-1 for different regions of the  
310 atmosphere. The tagging of CO sources includes both biomass burning (BB) and non-biomass burning (non-  
311 BB) from four continental areas, with all other sources put into the “other” bin. Other BB sources are small,  
312 but other non-BB sources are quite large as they include all natural sources as well as atmospheric  
313 photochemical sources such as methane oxidation.

314 Figure 5 shows the contribution of each tagged tracer over the Pacific Ocean from 120°E to 110°W,  
315 averaged over 5 degree latitude bins. Non-biomass burning sources dominate at all latitudes, due in part to  
316 the inclusion of CO from methane oxidation in addition to fossil fuel sources in these tracers. The oxidation  
317 of methane over the remote oceans contributes to the large magnitude of “other non-BB” sources over the  
318 southern latitudes of the Pacific. Asian non-BB sources make the largest contribution to middle and upper  
319 tropospheric CO (Fig. 5a) at the mid-latitudes of the North Pacific, with smaller contributions from N.  
320 American and European non-BB sources. The largest biomass burning contribution comes from Africa in  
321 the Southern Hemisphere and Tropics, switching to Eurasia in the northern latitudes.

322 Figure 5b shows the relative contributions in the lower troposphere, including the marine boundary  
323 layer and defined here as pressures greater than 850 hPa. Missing bars indicate latitudes where no ATom-1  
324 measurements were made in the lower troposphere. Asian non-BB CO makes a smaller contribution in the  
325 lower troposphere than in the middle and upper troposphere. A strong CO maximum around 30°N is more  
326 pronounced in the lower troposphere than above. This bin is not representative of the remote Pacific as it  
327 includes Palmdale, California, with large contributions from local North American BB and non-BB sources.

328 The Atlantic flights (0°-60°W) show a large contribution from other non-BB sources in the Southern  
329 Hemisphere with increasing contributions from Asian, N. American, and European non-BB CO as the flight  
330 moves northward (Fig. 6), similar to the picture over the Pacific. However, the Atlantic receives a larger  
331 contribution from biomass burning, particularly from Africa, over the Tropics. The contribution from African  
332 BB is strong throughout the troposphere, but is particularly pronounced in the lower troposphere, where it  
333 exceeds 100 ppb in the bins centered at 10°S and 5°N.

334 We also examine the tagged tracer contributions for each flight, including all altitudes sampled by  
335 the flight (Fig. 7, Supp. Table S1). Flights occurring in the tropics and southern hemisphere (Flt. 1, 4-8)

336 receive 44-75% of the total CO from other non-BB sources. Other non-biomass burning sources include all  
337 non-biomass burning sources located outside North America, Europe, and Asia. The contribution from  
338 methane oxidation in addition to southern hemisphere emissions explains this large contribution. Flight 8  
339 has a somewhat lower percent contribution from other non-BB sources than the other southern hemisphere  
340 and tropical flights due to the higher percent contribution from African biomass burning. In contrast, the  
341 Northern Hemisphere flights have a larger contribution from northern hemisphere source regions. Asian  
342 non-BB explains over a third of the total CO for the northern Pacific flights (Flt. 2-3), while Asian and N.  
343 American non-BB sources make comparable contributions to the North Atlantic and N. American flights (Flt.  
344 9-11).

345 Since Figs. 5 and 6 reveal differences in source contributions between the lower troposphere and the  
346 middle and upper troposphere, we also examine the source contributions to each flight for the lower  
347 troposphere (Pressure > 850 hPa) only (Supp. Fig. S7). Asian sources make a larger percent contribution to  
348 the Pacific flights (Flt. 0-4) when all flight altitudes are considered rather than the lower troposphere alone.  
349 Regional sources such as African biomass burning for flights 6 and 7 and N. American sources for Flights 9  
350 and 10 make a larger percent contribution in the lower troposphere.

Deleted: 5

## 351 5 August 2016 in the Context of Interannual Variability (IAV)

352 One of the major goals for the ATom campaign is to produce a climatology based on un-biased,  
353 representative samples (Prather *et al.*, 2017). It is therefore important to consider whether August 2016 is a  
354 “typical” boreal summer/austral winter month. Prather *et al.* [2018] found differences of 8-10% in the  
355 chemical reactivity of model simulated air parcels when considering other years compared to 2016. We focus  
356 here on the temporal representativeness of the ATom-1 campaign. Spatial representativeness is investigated  
357 in Liu *et al.* [in prep]. August of 2016 was ENSO neutral, with a multivariate ENSO index (MEI) (Wolter  
358 and Timlin, 1993); (<https://www.esrl.noaa.gov/psd/enso/mei>) of 0.175 for July/August. However, it was  
359 preceded by strong El Nino conditions in 2015 and early 2016 (Blunden and Arndt, 2016). We therefore  
360 consider whether the CO concentrations in August 2016 are typical or anomalous.

361 Multi-year satellite records provide a valuable tool for determining how CO concentrations in the  
362 regions of the ATom-1 flights compare to previous years. We focus our analysis of CO interannual  
363 variability on several regions traversed by the ATom flights. Figure 8 shows these regions in black squares  
364 overplotted on the MOPITT CO column for August 2016. We also examine the IAV in BB sources from  
365 nearby regions, outlined in red on Fig. 8. Figure 9 shows box-and-whisker plots of the mean, minimum, 25<sup>th</sup>,  
366 50<sup>th</sup>, and 75<sup>th</sup> percentiles, and maximum in monthly mean August CO for each region over the 2000-2016  
367 period for MOPITT (CO column and CO at 700 hPa) and 2004-2016 for MLS (CO at 215 hPa). The  
368 corresponding time series are shown in Fig. 10. The variability in CO BB emissions from the Global Fire  
369 Emissions Database version 4 (GFEDv4) (van der Werf *et al.*, 2017) for 2000-2016 is also shown for BB  
370 regions that may affect the ATom flights. The BB emissions are averaged over June through August to  
371 account for the persistence of CO in the atmosphere.

373 Among the regions mapped here, the tropical Atlantic shows the highest average CO values, as well  
374 as the highest 2016 CO values, in both MOPITT and MLS observations (Fig. 9). This is consistent with large  
375 biomass burning emissions from southern hemisphere (SH) Africa transported into the tropical Atlantic.  
376 While SH Africa has the largest magnitude of biomass burning, its relative variability (variability relative to  
377 the mean) is smaller than for the other regions (Fig. 9b). Similarly, the IAV in the MOPITT CO column and  
378 700 hPa level over tropical Atlantic is smaller than that of the North Atlantic and Alaska regions. Although  
379 the variability of CO over tropical Atlantic is relatively small, the MOPITT CO column shows a statistically  
380 significant anti-correlation between the MOPITT CO column over the tropical Atlantic and the MEI ( $r=-$   
381  $0.52$ ). This relationship is not significant for the MOPITT 700 hPa level.

382 The time series of August MOPITT CO columns for both the North Atlantic and Alaska, regions  
383 that show high variability, show a small but significant temporal correlation with summertime Siberian  
384 biomass burning ( $r=0.52$  for the North Atlantic and  $r=0.59$  for Alaska). Slightly lower values are seen for  
385 the 700 hPa MOPITT level. The time series of August MOPITT 700 hPa CO shows an increase in 2003 for  
386 the North Atlantic and in 2002 and 2003 for Alaska (Fig. 10b,c). Previous studies attribute peaks in these  
387 years to the presence of large forest fires in western Russia and Siberia, respectively (Edwards et al.,  
388 2004;Yashiro et al., 2009;van der Werf et al., 2006). MOPITT CO values were below average in 2016 for  
389 both the North Atlantic and Alaska even though Siberian biomass burning was above average in 2016 (Fig.  
390 9a, b).

391 Since ENSO is known to drive large biomass burning variability in Indonesia (*van der Werf et al.*,  
392 2006), we consider whether it may influence CO concentrations over the New Zealand region. Although the  
393 MOPITT CO column over the Indonesia region does correlate with the MEI ( $r=0.64$ ), there is no significant  
394 correlation between June-Aug biomass burning in Indonesia and MOPITT CO over New Zealand. However,  
395 August is not the peak season for Indonesian biomass burning (*Duncan et al.*, 2003b). The large Indonesian  
396 fires that occurred during the strong 1997/1998 El Nino peaked during September to November (*Duncan et*  
397 *al.*, 2003a) and active fire detections for the 2015 Indonesian fires peaked in September and October (*Field*  
398 *et al.*, 2016). Thus we might expect Indonesian biomass burning variability to have a greater influence on  
399 CO variability during the September-October season, which was sampled in ATom-3.

400 How does 2016 compare to previous years? The MOPITT CO column shows tropical Atlantic CO  
401 was near the 75<sup>th</sup> percentile, while the 700 hPa MOPITT level shows it close to the median. This difference  
402 arises because the MOPITT column also includes information from the upper troposphere, and the MOPITT  
403 200 hPa level (not shown) suggests CO levels for 2016 were near the 75<sup>th</sup> percentile. In contrast, MLS shows  
404 that 2016 CO in the upper troposphere was much lower than average, near the 25<sup>th</sup> percentile. The MOPITT  
405 v6 TIR product has a small positive bias drift in the upper troposphere of 0.78 % yr<sup>-1</sup> for the 200 hPa level  
406 (*Deeter et al.*, 2014), which may contribute to the higher rank of 2016 in the MOPITT upper tropospheric  
407 data compared to MLS. It is therefore hard to argue that 2016 was outside of the normal IAV for this region.

408 2016 CO in the North Atlantic and Alaska regions was below average in both the MOPITT column  
409 and the 700 hPa level, and is in fact the lowest August value in the MOPITT record for the 700 hPa level

Deleted: autumn

411 over Alaska. MLS also shows moderately low CO in the upper troposphere over Alaska in Aug. 2016.  
412 Combined, this data suggests that the ATom-1 CO is not typical for the region. August 2016 CO column  
413 values are also below the median over New Zealand and the eastern and central tropical Pacific, but the  
414 relatively low variability of these regions makes this less of a concern for the representativeness of the ATom  
415 measurements. The IAV of these regions is larger for the MOPITT 700 hPa level, and 2016 lies slightly  
416 below the 25<sup>th</sup> percentile for this level.

417 The regionally-averaged 500 nm AOT from MODIS (Fig. 11) shows similar features to the MOPITT  
418 column. The highest values are found for the tropical Atlantic, followed by the Alaska and North Atlantic  
419 regions. [This similarity is consistent with the importance of biomass burning emissions for both CO and](#)  
420 [aerosols](#). However, the difference between the tropical Atlantic and the other regions is larger in the aerosol  
421 case, while the difference between the North Atlantic and the Pacific regions is smaller. There is also greater  
422 relative year-to-year variability over the tropical Atlantic for the aerosols than for CO. The shorter lifetime  
423 of aerosols compared to CO, as well as the large contribution from biomass burning, likely explains the  
424 greater prominence of the tropical Atlantic in the aerosol case. Furthermore, AOD (Fig. 12) shows a clear  
425 peak in 2009 in several of the regions, whereas MOPITT data is missing for Aug. 2009, but MLS shows a  
426 minimum (Tropical Atlantic) or no anomaly (other regions).

427 In summary, the multi-year satellite record shows considerable variability in CO, particularly over the  
428 North Atlantic and Alaska. Concentrations during August 2016 were on the low end of the distribution for  
429 most regions, especially in the lower troposphere. *Worden et al. (2013)* showed negative trends in the  
430 MOPITT CO column significant at the one-sigma level for both the Northern and Southern hemispheres for  
431 2000-2012. In addition, *Deeter et al. (2014)* report a small negative bias drift in the MOPITT V6 TIR product  
432 in the lower troposphere, although drift in the column is almost negligible. Decreasing MOPITT CO over  
433 time is also visible in some regions in Fig. 10. This negative trend may be contributing to the low values in  
434 2016, [although there is also substantial IAV in CO](#). Overall, the year 2016 shows anomalies for some regions,  
435 but does not appear to be an extreme year.

## 436 6 Conclusions

437 We place the observations from the ATom-1 campaign in the context of interannual variability and  
438 global source distributions using satellite observations and tagged tracers from GEOS-5, respectively.  
439 GEOS-5 gives a reasonable reproduction of the background CO levels for most flights despite the use of  
440 climatological fossil fuel and biofuel emissions, and captures the global distribution of CO observed during  
441 ATom-1. Simulations with both forecast and analysis winds capture the timing of many of the enhanced CO  
442 plumes encountered during the flights, although the magnitude of the enhancements was often  
443 underestimated, which is not unexpected given the difference in resolution between the observations and  
444 model. The strong performance of GEOS-5 with regards to the overall CO distribution and the timing of the  
445 enhancements gives us confidence in using tagged tracers to identify the sources affecting the air sampled in  
446 ATom-1.



447 We find that for most flights the dominant contribution to total CO is from non-biomass burning  
448 sources, which include both fossil fuels and biofuels and oxidation of hydrocarbons including methane. An  
449 exception to this is in the lower troposphere of the tropical Atlantic, where biomass burning from Africa  
450 makes the largest contribution, exceeding 100 ppb in some locations. The non-BB source includes a large  
451 fraction from Asia for flights over the North Pacific and from both Asia and North America for the North  
452 Atlantic and North American flights, while other regions dominate in the Southern Hemisphere. Plumes of  
453 elevated CO from both biomass burning and non-BB sources led to observations of enhanced CO during  
454 ATom-1.

455 We use satellite observations of CO from MOPITT and MLS and AOT from MODIS to assess whether  
456 August 2016, the period sampled by ATom-1, is typical or atypical in the context of IAV in the satellite  
457 record (2000-2016). MOPITT and MLS show that CO in the lower and upper troposphere, respectively,  
458 were below average in August 2016 compared to the satellite record for August for most of the regions  
459 sampled by ATom-1, but not usually the minimum year. CO concentrations in the North Atlantic and Alaskan  
460 regions show a positive correlation with Siberian biomass burning and large interannual variability. In  
461 contrast, both MODIS AOT and the MOPITT CO column show above average values for the Tropical  
462 Atlantic in 2016. This suggests that the high values of CO and aerosols from biomass burning encountered  
463 during the tropical Atlantic portions of ATom may have been especially pronounced during this particular  
464 year.

465 The seasonality of biomass burning, the OH distribution, and atmospheric transport pathways can alter  
466 the source contributions from season to season. Thus, the next three ATom campaigns, which occur in  
467 different seasons, will likely show variations in the relative source contributions to each region.

468

#### 469 **Data Availability**

470 The QCLS data version used in this paper and the corresponding tagged-CO model output will be available  
471 from the ORNL DAAC at <https://doi.org/10.3334/ORNLDAAC/1604>. MOPITT data is available at  
472 <https://eosweb.larc.nasa.gov/datapool>. MLS data is available from <https://mls.jpl.nasa.gov/>. MODIS aerosol  
473 data are available from <https://ladsweb.modaps.eosdis.nasa.gov/api/v1/productGroupPage/name=aerosol>.

474

#### 475 **Acknowledgements**

476 The authors thank the NASA GMAO for providing the GEOS-5 forecasts and analyses. We thank the NASA  
477 Earth Venture Suborbital Program, ESPO, and the pilots, crew and support staff of the DC-8.

478

479

#### 480 **References**

481 ATom Science Team (2017), Moffett Field, CA, NASA Ames Earth Science Project Office (ESPO),  
482 Accessed at doi: 10.5067/Aircraft/ATom/TraceGas\_Aerosol\_Global\_Distribution

**Deleted:** Data from ATom-1 is available on the ESPO archive (<https://espo.nasa.gov/home/atom/archive/browse/atom>).

486 Bian, H., Colarco, P., Chin, M., Chen, G., Rodriguez, J., Liang, Q., Blake, D., Chu, D., da Silva, A.,  
487 Darmenov, A., Diskin, G., Fuelberg, H., Huey, G., Kondo, Y., Nielsen, J., Pan, X., and Wisthaler, A.: Source  
488 attributions of pollution to the Western Arctic during the NASA ARCTAS field campaign, *Atmospheric*  
489 *Chemistry and Physics*, 13, 4707-4721, 10.5194/acp-13-4707-2013, 2013.

490 e.d. Blunden, J., and D. S. Arndt: State of the Climate in 2015. In: *Bull. Amer. Meteor. Soc.*, 97(8), 2016.

491 Darmenov, A. and A. da Silva, The Quick Fire Emissions Dataset (QFED): Documentation of versions 2.1,  
492 2.2 and 2.4. NASA/TM-2015-104606, Vol. 38, 2015.

493 Deeter, M., Martinez-Alonso, S., Edwards, D., Emmons, L., Gille, J., Worden, H., Sweeney, C., Pittman, J.,  
494 Daube, B., and Wofsy, S.: The MOPITT Version 6 product: algorithm enhancements and validation,  
495 *Atmospheric Measurement Techniques*, 7, 3623-3632, 10.5194/amt-7-3623-2014, 2014.

496 Duncan, B., Bey, I., Chin, M., Mickley, L., Fairlie, T., Martin, R., and Matsueda, H.: Indonesian wildfires of  
497 1997: Impact on tropospheric chemistry, *Journal of Geophysical Research-Atmospheres*, 108,  
498 10.1029/2002JD003195, 2003a.

499 Duncan, B. N., Martin, R. V., Staudt, A. C., Yevich, R., and Logan, J. A.: Interannual and seasonal variability  
500 of biomass burning emissions constrained by satellite observations, *Journal of Geophysical Research-*  
501 *Atmospheres*, 108, 10.1029/2002jd002378, 2003b.

502 [Duncan, B. N., Logan, J. A., Bey, I., Megretskaja, I. A., Yantosca, R. M., Novelli, P. C., Jones, N. B., and](#)  
503 [Rinsland, C. P.: Global budget of CO, 1988-1997: Source estimates and validation with a global model, \*J.\*](#)  
504 [Geophys. Res. Atmos.](#), 112, 10.1029/2007JD008459, 2007.

505 Duncan, B. N., and Logan, J. A.: Model analysis of the factors regulating the trends and variability of carbon  
506 monoxide between 1988 and 1997, *Atmospheric Chemistry and Physics*, 8, 7389-7403, 2008.

507 [Eastham, S. D. and Jacob, D. J.: Limits on the ability of global Eulerian models to resolve intercontinental](#)  
508 [transport of chemical plumes, \*Atmos. Chem. Phys.\*, 17, 2543-2553, doi:10.5194/acp-17-2543-2017, 2017.](#)

509 Edwards, D., Petron, G., Novelli, P., Emmons, L., Gille, J., and Drummond, J.: Southern Hemisphere carbon  
510 monoxide interannual variability observed by Terra/Measurement of Pollution in the Troposphere  
511 (MOPITT), *Journal of Geophysical Research-Atmospheres*, 111, 10.1029/2006JD007079, 2006.

512 Edwards, D. P., Emmons, L. K., Hauglustaine, D. A., Chu, D. A., Gille, J. C., Kaufman, Y. J., Petron, G.,  
513 Yurganov, L. N., Giglio, L., Deeter, M. N., Yudin, V., Ziskin, D. C., Warner, J., Lamarque, J. F., Francis, G.  
514 L., Ho, S. P., Mao, D., Chen, J., Grechko, E. I., and Drummond, J. R.: Observations of carbon monoxide and  
515 aerosols from the Terra satellite: Northern Hemisphere variability, *Journal of Geophysical Research-*  
516 *Atmospheres*, 109, 10.1029/2004jd004727, 2004.

517 Emmons, L., Pfister, G., Edwards, D., Gille, J., Sachse, G., Blake, D., Wofsy, S., Gerbig, C., Matross, D.,  
518 and Nedelec, P.: Measurements of Pollution in the Troposphere (MOPITT) validation exercises during  
519 summer 2004 field campaigns over North America, *Journal of Geophysical Research-Atmospheres*, 112,  
520 10.1029/2006JD007833, 2007.

521 Field, R., van der Werf, G., Fanin, T., Fetzner, E., Fuller, R., Jethva, H., Levy, R., Livesey, N., Luo, M., Torres,  
522 O., and Worden, H.: Indonesian fire activity and smoke pollution in 2015 show persistent nonlinear

523 sensitivity to El Nino-induced drought, *Proceedings of the National Academy of Sciences of the United States*  
524 *of America*, 113, 9204-9209, 10.1073/pnas.1524888113, 2016.

525 Heald, C., Jacob, D., Fiore, A., Emmons, L., Gille, J., Deeter, M., Warner, J., Edwards, D., Crawford, J.,  
526 Hamlin, A., Sachse, G., Browell, E., Avery, M., Vay, S., Westberg, D., Blake, D., Singh, H., Sandholm, S.,  
527 Talbot, R., and Fuelberg, H.: Asian outflow and trans-Pacific transport of carbon monoxide and ozone  
528 pollution: An integrated satellite, aircraft, and model perspective, *Journal of Geophysical Research-*  
529 *Atmospheres*, 108, 10.1029/2003JD003507, 2003.

530 Hsu, J., Prather, M., Wild, O., Sundet, J., Isaksen, I., Browell, E., Avery, M., and Sachse, G.: Are the TRACE-  
531 P measurements representative of the western Pacific during March 2001?, *Journal of Geophysical Research-*  
532 *Atmospheres*, 109, 10.1029/2003JD004002, 2004.

533 Kasischke, E., Hyer, E., Novelli, P., Bruhwiler, L., French, N., Sukhinin, A., Hewson, J., and Stocks, B.:  
534 Influences of boreal fire emissions on Northern Hemisphere atmospheric carbon and carbon monoxide,  
535 *Global Biogeochemical Cycles*, 19, 10.1029/2004GB002300, 2005.

536 Langenfelds, R., Francey, R., Pak, B., Steele, L., Lloyd, J., Trudinger, C., and Allison, C.: Interannual growth  
537 rate variations of atmospheric CO<sub>2</sub> and its delta C-13, H-2, CH<sub>4</sub>, and CO between 1992 and 1999 linked to  
538 biomass burning, *Global Biogeochemical Cycles*, 16, 10.1029/2001GB001466, 2002.

539 Levy, R., Hsu, C., et al.: MODIS Atmosphere L2 Aerosol Product. NASA MODIS Adaptive Processing  
540 System, Goddard Space Flight Center, USA, doi:[http://dx.doi.org/10.5067/MODIS/MYD04\\_L2.006](http://dx.doi.org/10.5067/MODIS/MYD04_L2.006), 2015.

541 Liu, J., J. A. Logan, L. T. Murray, H. C. Pumphrey, and I. A. Megretskaja, Transport analysis and source  
542 attribution of seasonal and interannual variability of CO in the tropical upper troposphere and lower  
543 stratosphere. *Atmos. Chem. Phys.*, **13**: 129-146 doi:[10.5194/acp-13-129-2013](https://doi.org/10.5194/acp-13-129-2013), 2013.

544 Livesey, N., Filipiak, M., Froidevaux, L., Read, W., Lambert, A., Santee, M., Jiang, J., Pumphrey, H., Waters,  
545 J., Cofield, R., Cuddy, D., Daffer, W., Drouin, B., Fuller, R., Jarnot, R., Jiang, Y., Knosp, B., Li, Q., Perun,  
546 V., Schwartz, M., Snyder, W., Stek, P., Thurstans, R., Wagner, P., Avery, M., Browell, E., Cammas, J.,  
547 Christensen, L., Diskin, G., Gao, R., Jost, H., Loewenstein, M., Lopez, J., Nedelec, P., Osterman, G., Sachse,  
548 G., and Webster, C.: Validation of Aura Microwave Limb Sounder O-3 and CO observations in the upper  
549 troposphere and lower stratosphere, *Journal of Geophysical Research-Atmospheres*, 113,  
550 10.1029/2007JD008805, 2008.

551 Logan, J., Megretskaja, I., Nassar, R., Murray, L., Zhang, L., Bowman, K., Worden, H., and Luo, M.: Effects  
552 of the 2006 El Nino on tropospheric composition as revealed by data from the Tropospheric Emission  
553 Spectrometer (TES), *Geophysical Research Letters*, 35, 10.1029/2007GL031698, 2008.

554 Lucchesi, R, File Specification for GEOS-5 FP. GMAO Office Note No. 4 (Version 1.1), 61pp, 2017,  
555 available from [http://gmao.gsfc.nasa.gov/pubs/office\\_notes](http://gmao.gsfc.nasa.gov/pubs/office_notes).

556 Molod, A., Takacs, L., Suarez, M., and Bacmeister, J.: Development of the GEOS-5 atmospheric general  
557 circulation model: evolution from MERRA to MERRA2, *Geoscientific Model Development*, 8, 1339-1356,  
558 10.5194/gmd-8-1339-2015, 2015.

559 Novelli, P., Masarie, K., Lang, P., Hall, B., Myers, R., and Elkins, J.: Reanalysis of tropospheric CO trends:  
560 Effects of the 1997-1998 wildfires, *Journal of Geophysical Research-Atmospheres*, 108,  
561 10.1029/2002JD003031, 2003.

562 Ott, L., Duncan, B., Pawson, S., Colarco, P., Chin, M., Randles, C., Diehl, T., and Nielsen, E.: Influence of  
563 the 2006 Indonesian biomass burning aerosols on tropical dynamics studied with the GEOS-5 AGCM,  
564 *Journal of Geophysical Research-Atmospheres*, 115, 10.1029/2009jd013181, 2010.

565 Pfister, G., Emmons, L., Edwards, D., Arellano, A., Sachse, G., and Campos, T.: Variability of springtime  
566 transpacific pollution transport during 2000-2006: the INTEX-B mission in the context of previous years,  
567 *Atmospheric Chemistry and Physics*, 10, 1345-1359, 10.5194/acp-10-1345-2010, 2010.

568 Prather, M., Zhu, X., Flynn, C., Strode, S., Rodriguez, J., Steenrod, S., Liu, J., Lamarque, J., Fiore, A.,  
569 Horowitz, L., Mao, J., Murray, L., Shindell, D., and Wofsy, S.: Global atmospheric chemistry - which air  
570 matters, *Atmospheric Chemistry and Physics*, 17, 9081-9102, 10.5194/acp-17-9081-2017, 2017.

571 Reinecker, M. M. et al., The GEOS-5 Data Assimilation System – Documentation of Versions 5.0.1, 5.1.0,  
572 and 5.2.0, Technical Report Series on Global Modeling and Data Assimilation, Vol. 27, ed. M. J. Suarez,  
573 NASA/TM-2008-104606, 2008.

574 [Prather, M. J., Flynn, C. M., Zhu, X., Steenrod, S. D., Strode, S. A., Fiore, A. M., Correa, G., Murray, L. T.,  
575 and Lamarque, J.-F.: How well can global chemistry models calculate the reactivity of short-lived greenhouse  
576 gases in the remote troposphere, knowing the chemical composition, \*Atmos. Meas. Tech.\*, 11, 2653-2668,  
577 <https://doi.org/10.5194/amt-11-2653-2018>, 2018.](#)

578 Rienecker, M. M., Suarez, M. J., Gelaro, R., Todling, R., Bacmeister, J., Liu, E., Bosilovich, M. G., Schubert,  
579 S. D., Takacs, L., Kim, G.-K., Bloom, S., Chen, J., Collins, D., Conaty, A., da Silva, A., Gu, W., Joiner, J.,  
580 Koster, R. D., Lucchesi, R., Molod, A., Owens, T., Pawson, S., Pegion, P., Redder, C. R., Reichle, R.,  
581 Robertson, F. R., Ruddick, A. G., Sienkiewicz, M., and Woollen, J.: MERRA: NASA's Modern-Era  
582 Retrospective Analysis for Research and Applications, *Journal of Climate*, 24, 3624-3648, 10.1175/JCLI-D-  
583 11-00015.1, 2011.

584 Santoni, G., Daube, B., Kort, E., Jimenez, R., Park, S., Pittman, J., Gottlieb, E., Xiang, B., Zahniser, M.,  
585 Nelson, D., McManus, J., Peischl, J., Ryerson, T., Holloway, J., Andrews, A., Sweeney, C., Hall, B., Hints,  
586 E., Moore, F., Elkins, J., Hurst, D., Stephens, B., Bent, J., and Wofsy, S.: Evaluation of the airborne quantum  
587 cascade laser spectrometer (QCLS) measurements of the carbon and greenhouse gas suite - CO<sub>2</sub>, CH<sub>4</sub>, N<sub>2</sub>O,  
588 and CO - during the CalNex and HIPPO campaigns, *Atmospheric Measurement Techniques*, 7, 1509-1526,  
589 10.5194/amt-7-1509-2014, 2014.

590 Strode, S. A., and Pawson, S.: Detection of carbon monoxide trends in the presence of interannual variability,  
591 *Journal of Geophysical Research-Atmospheres*, 118, 12257-12273, 10.1002/2013JD020258, 2013.

592 van der Werf, G., Randerson, J., Giglio, L., Collatz, G., Kasibhatla, P., and Arellano, A.: Interannual  
593 variability in global biomass burning emissions from 1997 to 2004, *Atmospheric Chemistry and Physics*, 6,  
594 3423-3441, 2006.

595 [van der Werf, G. R., Randerson, J. T., Giglio, L., van Leeuwen, T. T., Chen, Y., Rogers, B. M., Mu, M., van](#)  
596 [Marle, M. J. E., Morton, D. C., Collatz, G. J., Yokelson, R. J., and Kasibhatla, P. S.: Global fire emissions](#)  
597 [estimates during 1997–2016, Earth Syst. Sci. Data, 9, 697-720, <https://doi.org/10.5194/essd-9-697-2017>,](#)  
598 [2017.](#)

599 Voulgarakis, A., Marlier, M., Faluvegi, G., Shindell, D., Tsigaridis, K., and Mangeon, S.: Interannual  
600 variability of tropospheric trace gases and aerosols: The role of biomass burning emissions, *Journal of*  
601 *Geophysical Research-Atmospheres*, 120, 7157-7173, 10.1002/2014JD022926, 2015.

602 Waters, J., Froidevaux, L., Harwood, R., Jarnot, R., Pickett, H., Read, W., Siegel, P., Cofield, R., Filipiak,  
603 M., Flower, D., Holden, J., Lau, G., Livesey, N., Manney, G., Pumphrey, H., Santee, M., Wu, D., Cuddy, D.,  
604 Lay, R., Loo, M., Perun, V., Schwartz, M., Stek, P., Thurstans, R., Boyles, M., Chandra, K., Chavez, M.,  
605 Chen, G., Chudasama, B., Dodge, R., Fuller, R., Girard, M., Jiang, J., Jiang, Y., Knosp, B., LaBelle, R., Lam,  
606 J., Lee, K., Miller, D., Oswald, J., Patel, N., Pukala, D., Quintero, O., Scaff, D., Van Snyder, W., Tope, M.,  
607 Wagner, P., and Walch, M.: The Earth Observing System Microwave Limb Sounder (EOS MLS) on the Aura  
608 satellite, *Ieee Transactions on Geoscience and Remote Sensing*, 44, 1075-1092,  
609 10.1109/TGRS.2006.873771, 2006.

610 Wolter, K., and Timlin, M. S.: Monitoring ENSO in COADS with a seasonally adjusted principal component  
611 index, *Proc. of the 17th Climate Diagnostics Workshop*, 1993,

612 Worden, H. M., Deeter, M. N., Frankenberg, C., George, M., Nichitiu, F., Worden, J., Aben, I., Bowman, K.  
613 W., Clerbaux, C., Coheur, P. F., de Laat, A. T. J., Detweiler, R., Drummond, J. R., Edwards, D. P., Gille, J.  
614 C., Hurtmans, D., Luo, M., Martinez-Alonso, S., Massie, S., Pfister, G., and Warner, J. X.: Decadal record  
615 of satellite carbon monoxide observations, *Atmospheric Chemistry and Physics*, 13, 837-850, 10.5194/acp-  
616 13-837-2013, 2013.

617 Yashiro, H., Sugawara, S., Sudo, K., Aoki, S., and Nakazawa, T.: Temporal and spatial variations of carbon  
618 monoxide over the western part of the Pacific Ocean, *Journal of Geophysical Research-Atmospheres*, 114,  
619 10.1029/2008JD010876, 2009.

620 Ziemke, J., and Chandra, S.: La Nina and El Nino-induced variabilities of ozone in the tropical lower  
621 atmosphere during 1970-2001, *Geophysical Research Letters*, 30, 10.1029/2002GL016387, 2003.

622

623 **Table 1 : Regional August 2016 CO Emission Totals in the GEOS-5 FP Simulations**

	<b>Fossil Fuel<sup>1</sup></b>	<b>Biogenic<sup>1</sup></b>	<b>BB<sup>1</sup></b>
North America	6.7 (8.0)	5.8	2.4 (2.7)
Europe	4.9 (5.9)	2.4	
Asia	26 (31)	7.9	
Eurasia <sup>2</sup>			3.0 (3.3)
Africa			24 (27)
South America	13 (16)	17	11 (12)
Other <sup>3</sup>			2.9 (3.2)
Global	50 (60)	34	43 (48)

624 <sup>1</sup>Emissions are in units of Tg. Values in parentheses include the 20% and 11% scaling factors for fossil fuels  
625 and biomass burning, respectively, to account for CO production from VOC oxidation.

626 <sup>2</sup>The Eurasian tagged tracer for BB CO includes emissions from Europe and northern Asia, but excludes  
627 southern Asia.

628 <sup>3</sup>Other fossil fuel emissions includes emissions from Africa and South America, while other BB emissions  
629 excludes those regions since they are tagged separately. Other BB does include southern Asia as well  
630 Australia.

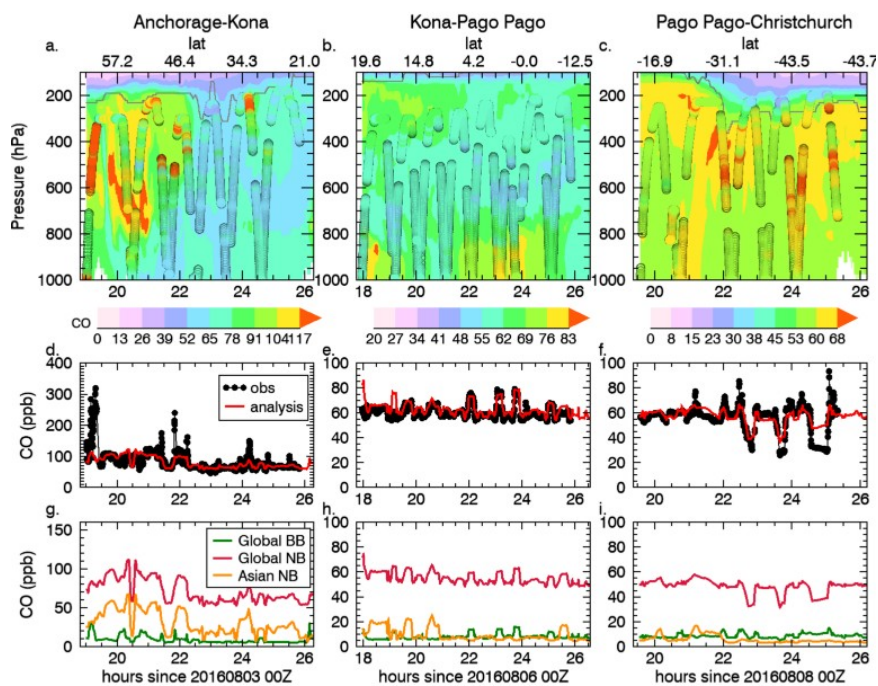
631

632 **Table 2: Mean and Standard Deviations in CO along Atlantic and Pacific Flight Tracks**

<b>Region</b>	<b>Flight</b>	<b>Obs Mean (ppb)</b>	<b>Obs Stdev (ppb)</b>	<b>Model Mean (ppb)</b>	<b>Model Stdev (ppb)</b>
Eastern Pacific	1. Palmdale – Palmdale	75	14	77	19
	2. Palmdale - Anchorage	100	40	88	16
Pacific	3. Anchorage-Kona	85	36	81	18
	4. Kona –Pago Pago	61	5.1	63	5.5
	5. Pago Pago – Christchurch	55	11	57	6.1
Southern Ocean	6. Christchurch – Punta Arenas	56	6.4	54	4.7
Atlantic	7. Punta Arenas – Ascension	69	17	71	26
	8. Ascension – Azores	101	36	103	27

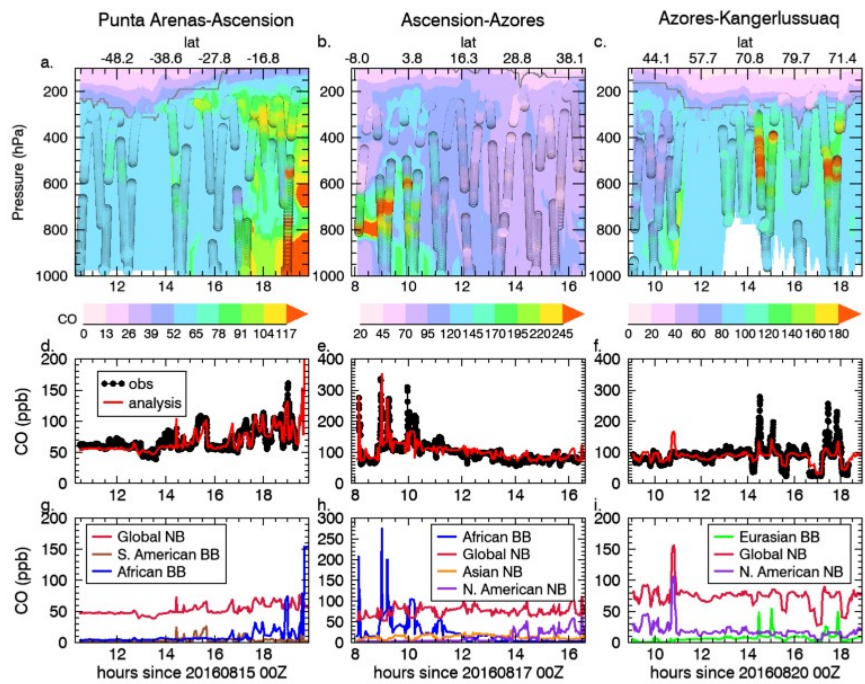
	9. Azores – Kangerlussuaq	88	32	87	19
N. America	10. Kangerlussuaq – Minneapolis	90	26	91	22
	11. Minneapolis – Palmdale	84	38	107	78

633  
634  
635  
636



637

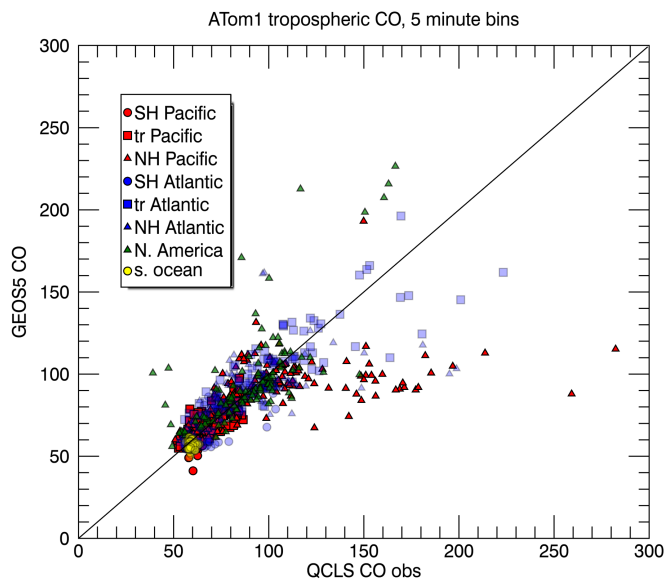
638 Figure 1: Curtian plot of CO (ppb) from the GEOS-5 analysis as a function of time and pressure overplotted with  
639 the model tropopause (gray line) and QCLS CO observations (circles) (top row) for the a) Anchorage to Kona  
640 flight, b) Kona to Pago Pago flight, and c) Pago Pago to Christchurch flight. Axis ranges vary between panels due  
641 to the large range of concentrations encountered. The top x-axis indicates the latitudes of the flight track. d-f)  
642 The GEOS-5 CO interpolated to the flight track (red line) is compared to the observations (black circles). g-h)  
643 Tagged tracer contributions to the GEOS-5 CO.



644

645 Figure 2: As in Fig. 1, but for the Atlantic flights: a,d,g) Punta Arenas-Ascension Island, b,e,h) Ascension Island  
 646 to the Azores, and c,f,i) Azores to Kangerlussuaq.

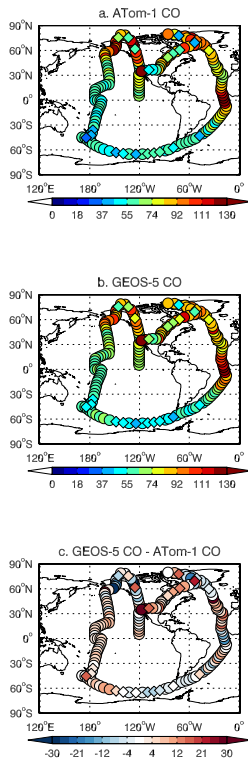




647

648 **Figure 3: GEOS-5 simulated CO versus QCLS CO observations for all ATom-1 flights averaged into 5 minute**  
 649 **bins. CO is in units of ppb. Pacific flights are shown in red, Atlantic flights in blue, N. American flights in green,**  
 650 **and southern ocean flights in yellow. Circles indicate Southern Hemisphere points, triangles indicate Northern**  
 651 **Hemisphere points, and squares indicate tropical points. The one-to-one line is overplotted in black.**

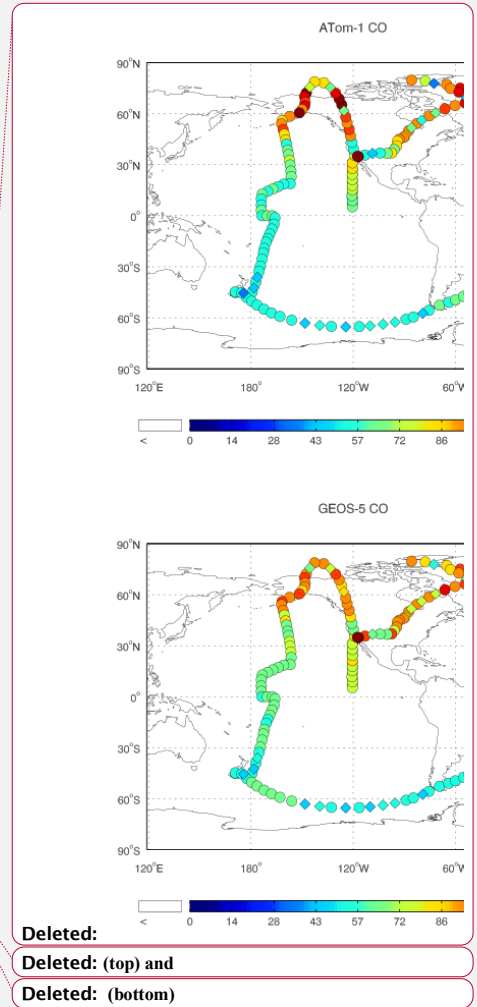
652

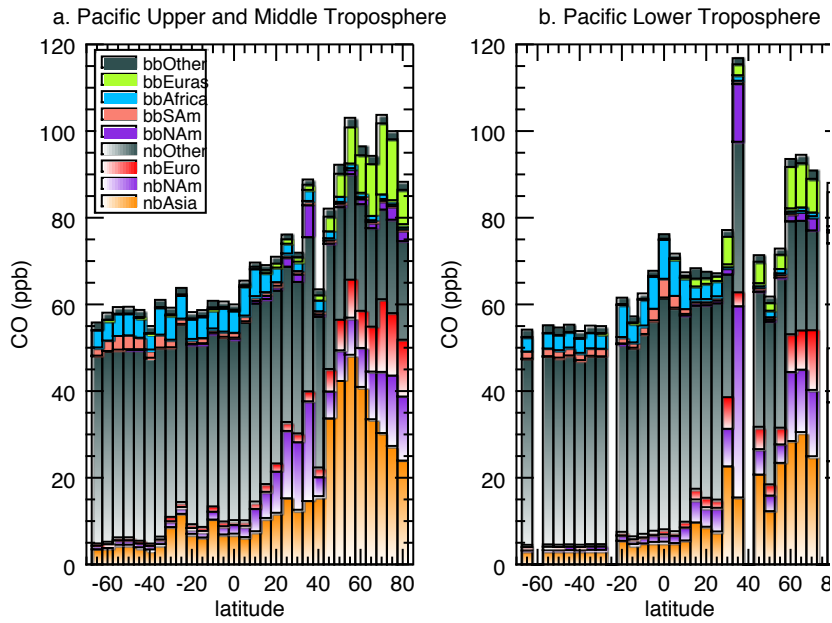


653

654 **Figure 4: CO (ppb) from the (a) QCLS observations, (b) GEOS-5 analysis, and (c) the GEOS-5 – obs difference**  
 655 **for the ATom-1 circuit including all 11 research flight segments. The GEOS-5 CO is taken from the analysis**  
 656 **closest to the mid-point of the flight time and interpolated to the flight track following the longitude, latitude and**  
 657 **pressure given in the observations. Both model forecast and ATom measurements are averaged into a sample rate**  
 658 **of one per 360-second. Data in the troposphere are plotted in a circle, while data in the stratosphere are plotted in**  
 659 **a diamond, based on the GEOS-5 tropopause.**

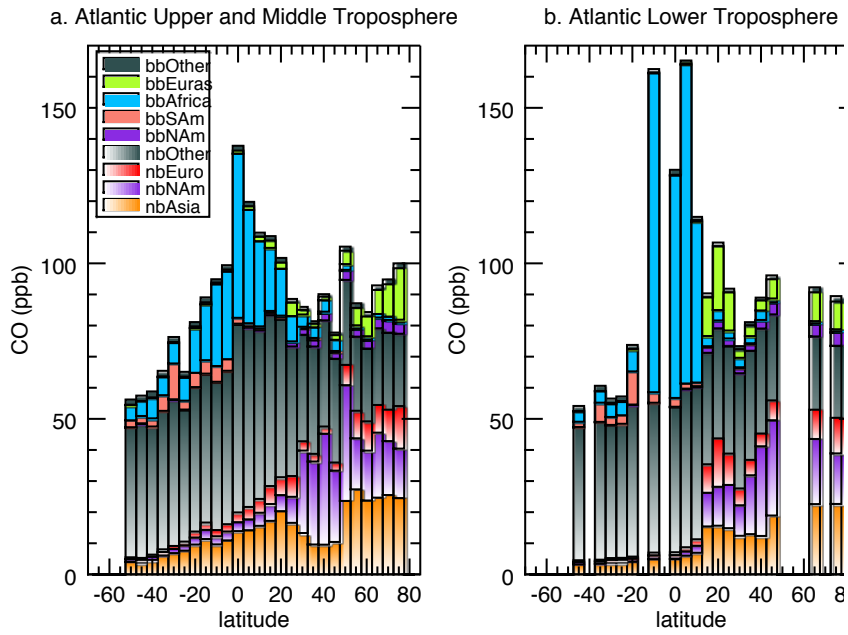
660





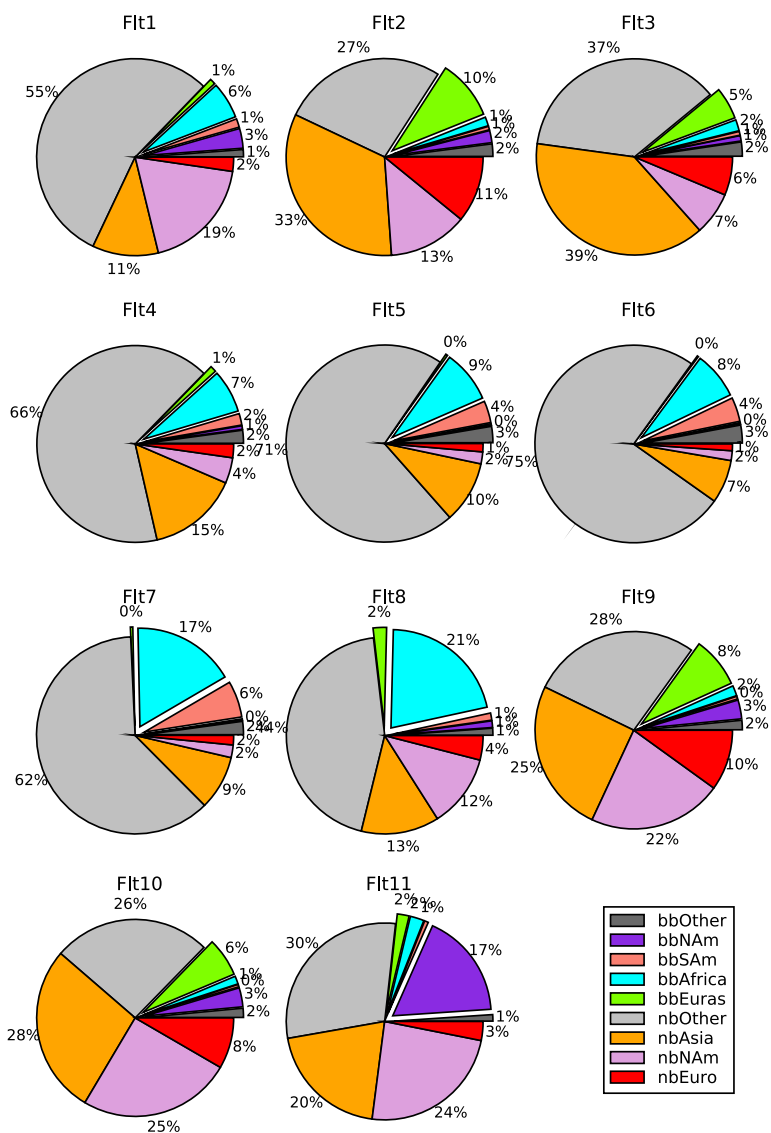
664

665 Figure 5: The contribution of each tagged CO tracer over the Pacific in the (a) upper and middle troposphere  
 666 (pressure  $\leq 850$  hPa) and (b) lower troposphere (pressure  $> 850$  hPa). Data from multiple flights over the region  
 667 between  $120^{\circ}\text{E}$  and  $110^{\circ}\text{W}$  is included, with each bar representing data averaged over a 5 degree latitude bin.  
 668 Shaded bars represent non-BB CO from Asia (orange), N. America (purple), Europe (red), and the rest of the  
 669 world (gray). Solid bars represent BB CO from N. America (purple), S. America (pink), Africa (cyan), Eurasia  
 670 (green), and the rest of the world (gray).



671

672 Figure 6: As in Fig. 5, but for the Atlantic. Data from multiple flights over the region 0-60°W is included, with  
 673 each bar representing data averaged over a 5 degree latitude bin.

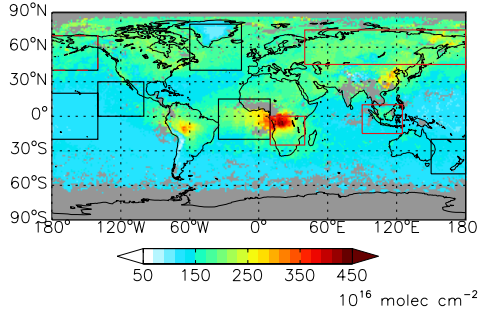


674

675 **Figure 7: Percent contributions of tagged tracers to total CO for each flight. Exploded slices represent the biomass**  
 676 **burning tracers: North American (purple), S. American (salmon), African (cyan), Eurasian (green), and Other**

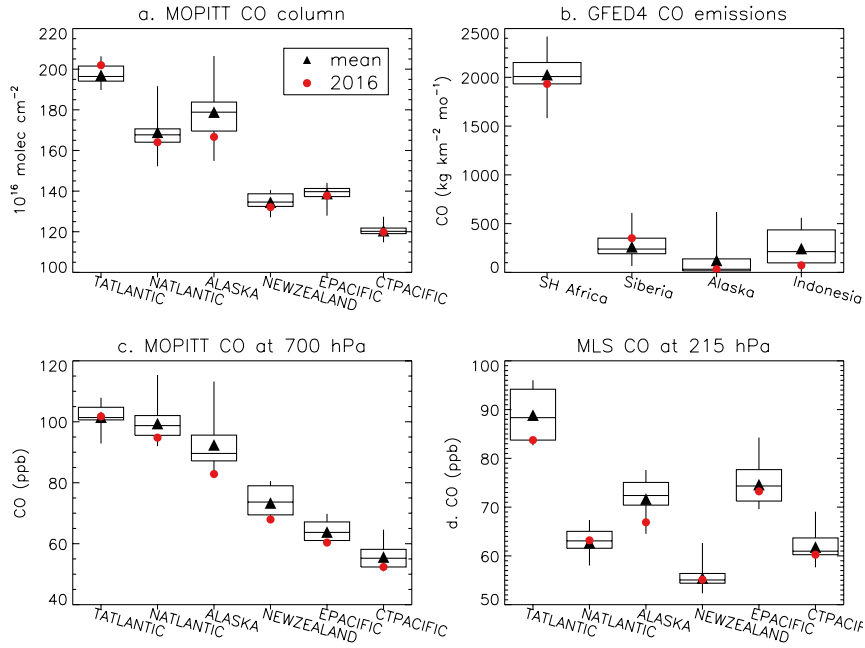
677 (dark gray). The non-biomass burning (nb) tracers are for Asia (orange), N. America (lavender), Europe (red),  
 678 and other (light gray).

679



680

681 **Figure 8: MOPITT CO column for August 2016 overlotted with the regions shown in Fig. 10. Black rectangles**  
 682 **indicate the regions where we analyze CO concentrations, and red rectangles indicate the regions used for biomass**  
 683 **burning.**

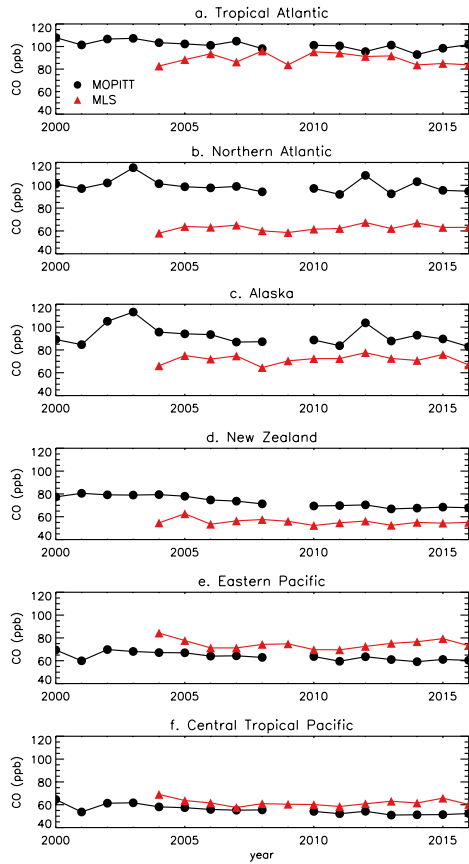


684

Deleted: ¶

Deleted: ¶

687 **Figure 9:** Boxes show the 25<sup>th</sup>, 50<sup>th</sup>, and 75<sup>th</sup> percentile values; whiskers show the minimum and maximum values;  
 688 black triangles show the mean value, and red circles show the 2016 value for a) the MOPITT CO column, b) the  
 689 GFED4 CO emissions, c) MOPITT CO at 700 hPa, and d) MLS CO at 215 hPa. Statistics for MOPITT are for  
 690 2000-2016, statistics for GFED4 are for 2000-2015, and statistics for MLS are for 2004-2016. MOPITT and MLS  
 691 values are for August, while the GFED4 emissions are averaged over June through August.

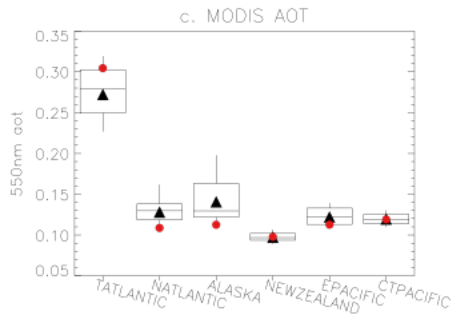


692

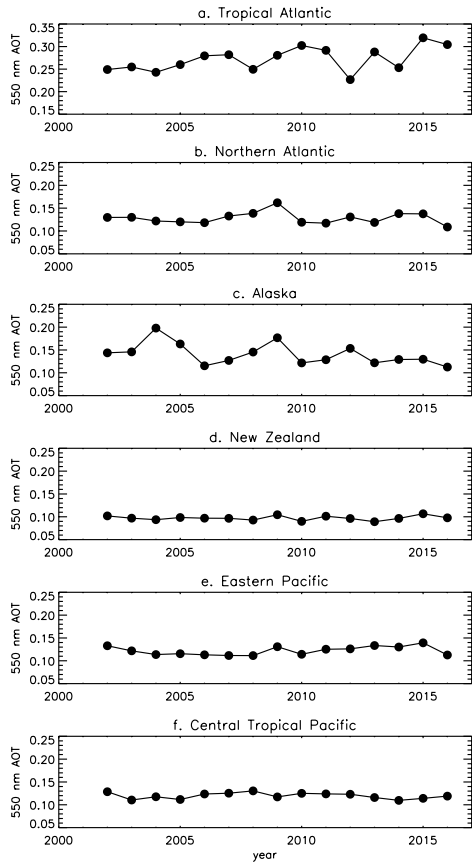
693

694 **Figure 10:** Time series of August MOPITT CO at the 700 hPa level (black circles) and MLS CO (red triangles)  
 695 at the 215 hPa level for the 6 regions shown in black in Fig. 8.

696



697 **Figure 11:** As in Figure 9, but for the August MODIS 550 nm AOT. Only values over oceans are included in the  
698 regional averages.



699 **Figure 12:** Time series of regionally averaged August MODIS 550 nm AOT. Only values over oceans are included  
700



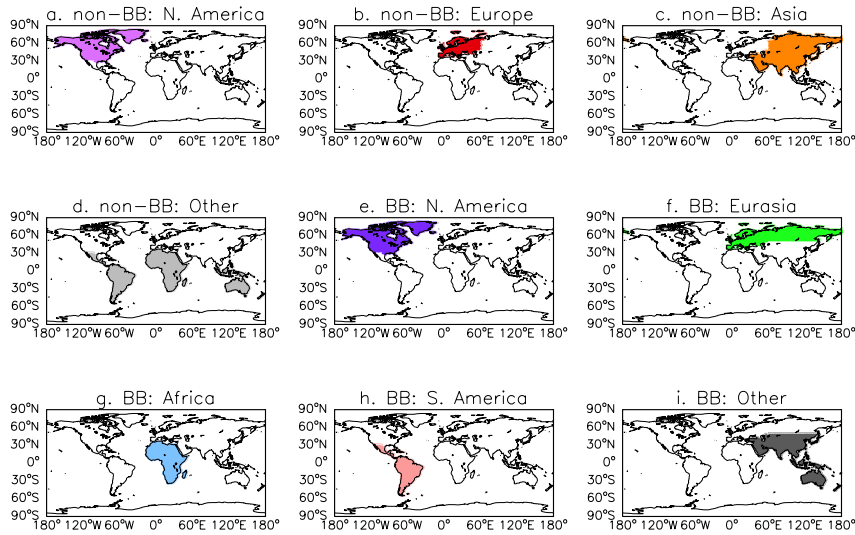
701 in the regional averages. The y-axis range for panel a differs from the other panels due to the higher AOT values  
702 in that region  
703

704 **Table S1: Tagged tracer contributions (ppbv) to CO from GEOS-5 averaged over each ATom-1 Flight. The**  
 705 **columns represent total CO (totCO), other BB (bbot), N. American BB (bbna), S. American BB (bbsa), African**  
 706 **bb (bbaf), Eurasian BB (bbea), other non-BB (nbot), Asian non-BB (nbas), N. American non-BB (nbna), and**  
 707 **European non-BB (nbeu).**

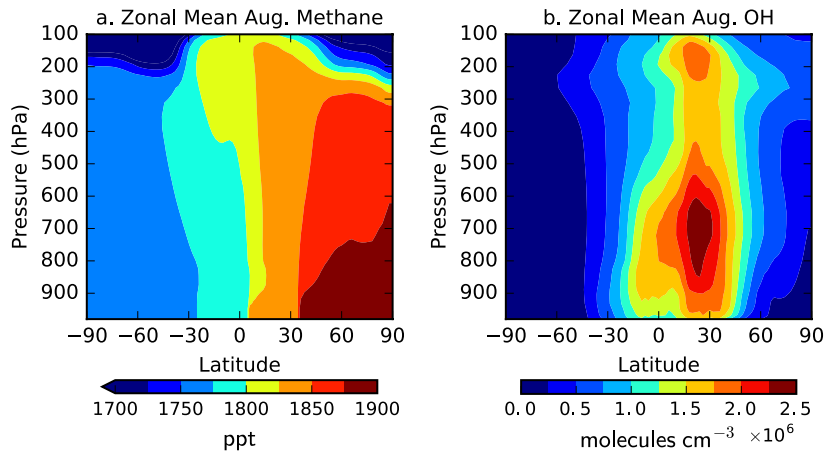
708

<b>flight</b>	<b>totCO</b>	<b>bbot</b>	<b>bbna</b>	<b>bbsa</b>	<b>bbaf</b>	<b>bbea</b>	<b>nbot</b>	<b>nbas</b>	<b>nbna</b>	<b>nbeu</b>
1	77.3	0.910	2.50	1.08	4.66	0.722	42.7	8.38	14.6	1.79
2	87.7	1.79	1.74	0.506	1.29	8.61	23.7	29.1	11.4	9.54
3	81.1	1.89	0.712	0.504	1.49	4.29	29.9	31.4	5.76	5.12
4	63.1	1.34	0.368	1.20	4.45	0.644	41.5	9.43	2.66	1.42
5	57.0	1.52	0.162	2.04	4.88	0.189	40.4	5.79	1.12	0.768
6	54.2	1.59	0.134	2.15	4.18	0.112	40.7	3.86	0.864	0.594
7	71.0	1.54	0.199	4.24	12.0	0.284	43.8	6.33	1.47	1.11
8	103	1.18	1.12	1.21	21.8	2.28	45.7	13.2	12.3	4.12
9	86.6	1.34	2.68	0.397	1.46	7.19	24.0	21.9	19.1	8.63
10	91.2	1.37	2.85	0.367	1.21	5.80	23.7	25.4	23.0	7.64
11	107	1.14	18.6	0.678	2.44	2.09	31.7	21.7	25.7	3.34

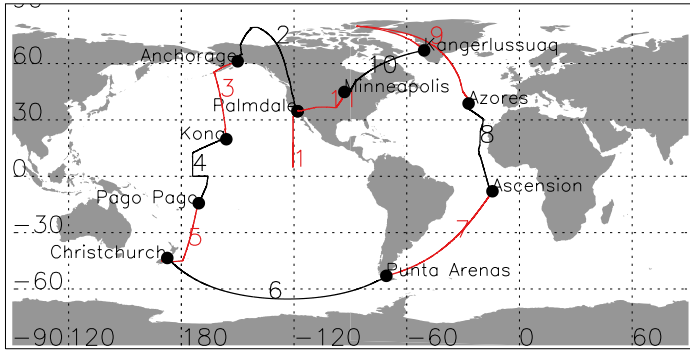
709  
710



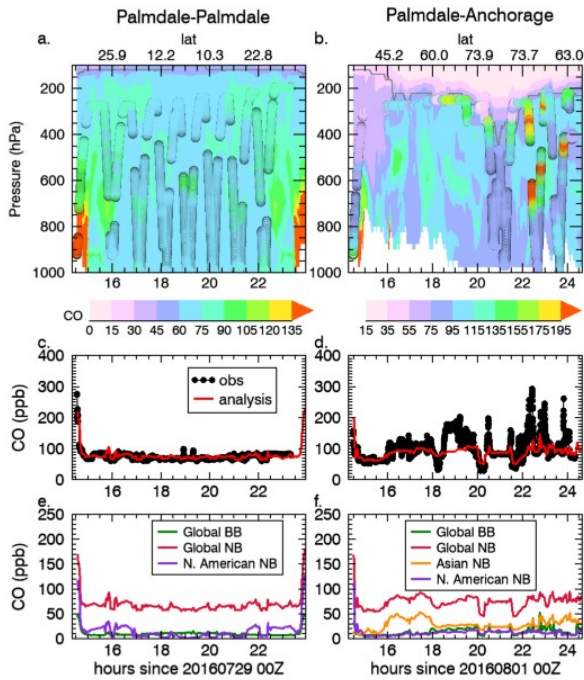
711  
 712 **Fig. S1: The regions corresponding to each tagged-CO tracer**  
 713



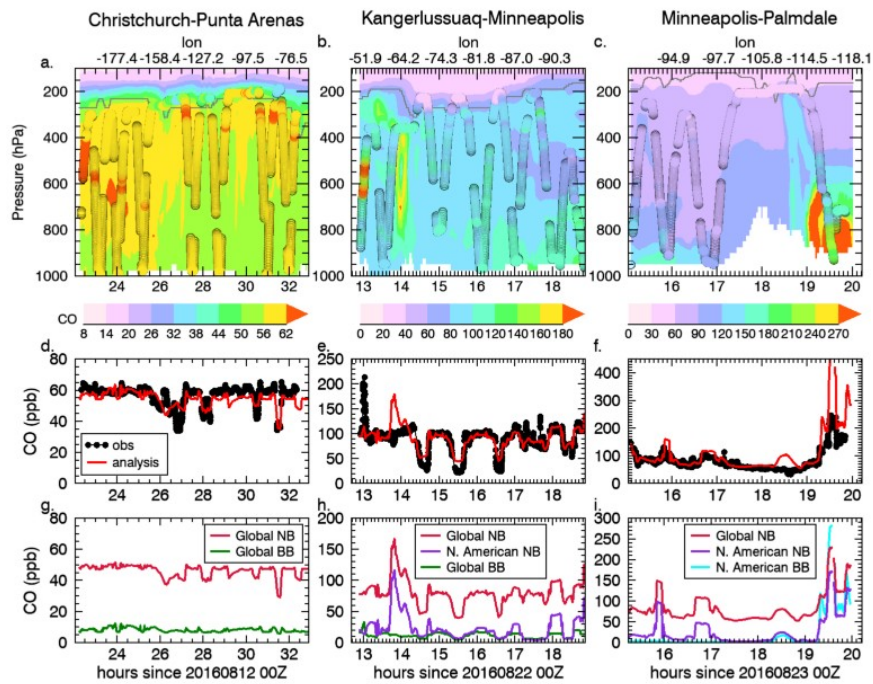
714  
 715 **Fig. S2: The August zonal mean (a) methane concentrations and (b) OH concentrations used in the GEOS-5 FP**  
 716 **CO simulation.**



717  
 718 **Fig. S3: The ATom-1 flight tracks. Labeled circles indicate the starting and ending points of each flight.**  
 719



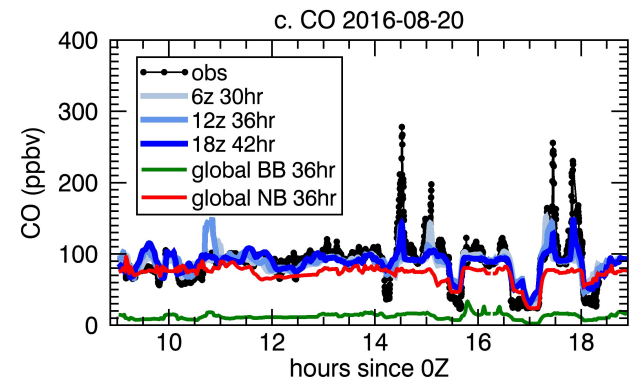
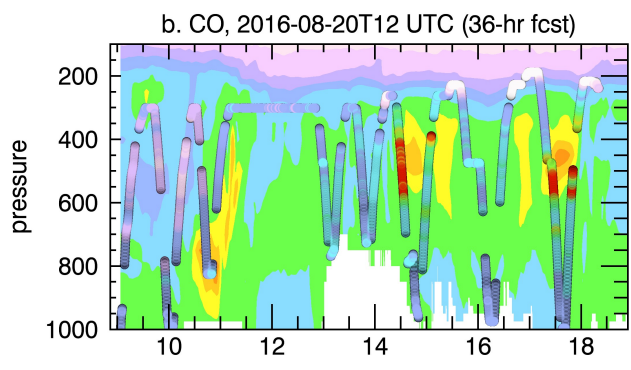
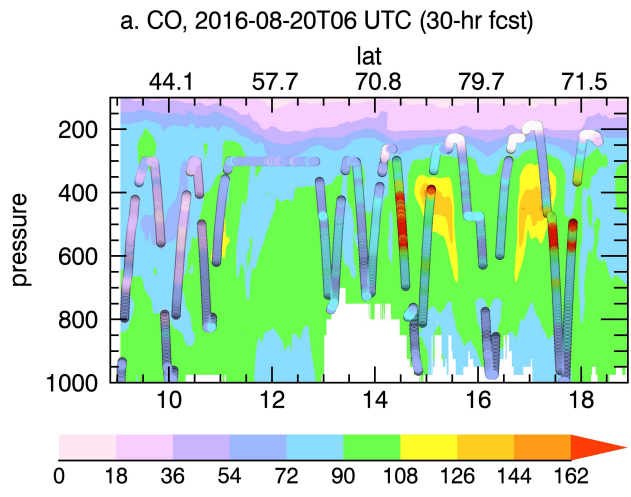
720  
 721 **Fig. S4: Curtain plot of CO (ppb) from the GEOS-5 analysis as a function of time and pressure overplotted with**  
 722 **QCLS CO observations (top row) for the a) Palmdale to Palmdale flight and b) Palmdale to Anchorage flight.**  
 723 **The top x-axis indicates the latitudes of the flight track. c-d) The GEOS-5 CO interpolated to the flight track (red**  
 724 **line) is compared to the observations (black circles). e-f) Tagged tracer contributions to the GEOS-5 CO.**



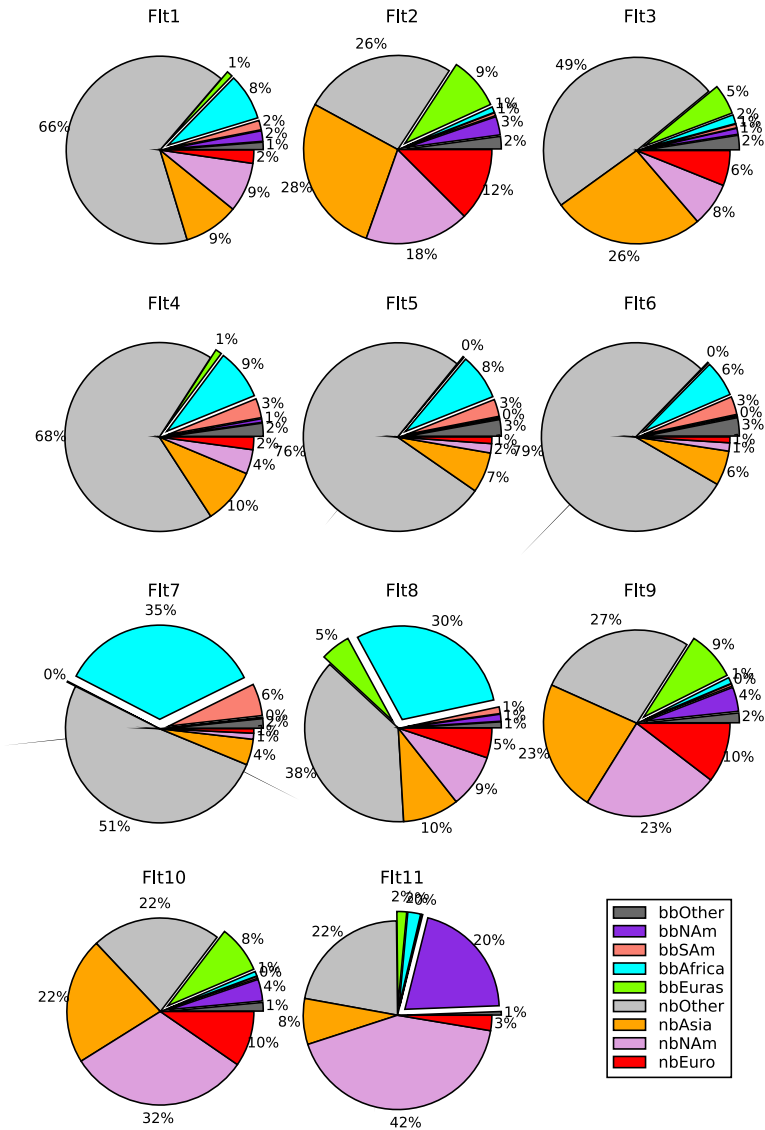
725

726 Fig. S5: Curtain plot of CO (ppb) from the GEOS-5 analysis as a function of time and pressure overplotted with  
 727 QCLS CO observations (top row) for the a) Christchurch to Punta Arenas flight, b) Kangerlussuaq to Minneapolis  
 728 flight, and c) Minneapolis to Palmdale flight. Axis ranges vary between panels due to the large range of  
 729 concentrations encountered. The top x-axis indicates the longitudes of the flight track. d-f) The GEOS-5 CO  
 730 interpolated to the flight track (red line) is compared to the observations (black circles). g-h) Tagged tracer  
 731 contributions to the GEOS-5 CO.

732



734 **Figure S6: Color contours of the GEOS-5 forecasted CO along the flight path of RF09 from Azores to**  
735 **Kangerlussuaq. The 30-hr forecast at 2016-08-20T6:00 (top) is compared with the 36-hr forecast (2016-08-**  
736 **20T12:00, middle). The ATom CO observations (circles) are pasted on both of these forecasts. (Bottom) time**  
737 **series of observed (black) and forecasted CO (blue) at different snap shot times (2016-08-20T6:00, 2016-08-**  
738 **20T12:00, 2016-08-20T18:00). It also shows the CO from global non-BB emissions (NB, red) and global biomass**  
739 **burning emissions (green).**



740

741 **Fig. S7: Percent contributions of tagged tracers to total CO in the lower troposphere for each flight. Exploded**  
 742 **slices represent the biomass burning tracers: North American (purple), S. American (salmon), African (cyan),**



743 Eurasian (green), and Other (dark gray). The non-biomass burning (nb) tracers are for Asia (orange), N. America  
744 (lavender), Europe (red), and other (light gray).  
745